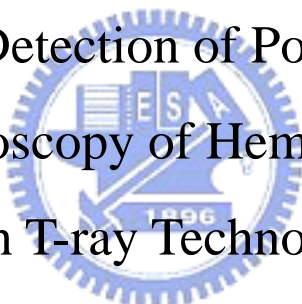# 國 立 交 通 大 學
光 電 工 程 研 究 所
碩 士 論 文

兆赫技術應用於豬皮燒傷深度的檢驗及

血紅素光譜量測

Burn-Depth Detection of Porcine Skin and

Spectroscopy of Hemoglobin

with T-ray Technology

研 究 生：吳 勝 隆

指 導 老 師：潘 犀 靈 教授

中 華 民 國 九 十 四 年 七 月

兆赫技術應用於豬皮燒傷深度的檢驗及

血紅素光譜量測

Burn-Depth Detection of Porcine Skin and

Spectroscopy of Hemoglobin

with T-ray Technology

研究生： 吳勝隆　　　　　　　　Student: Sheng-Lung Wu

指導老師：潘犀靈 教授　　　　　Advisor: Prof. Ci-Ling Pan

國 立 交 通 大 學

光 電 工 程 研 究 所

碩 士 論 文

A Dissertation
Submitted to Department of Photonics and Institute of Electro-Optic
Engineering
College of Electrical Engineering
National Chiao Tung University
In partial Fulfillment of the Requirements
for the Degree of
Master of Engineering

July 2005
Hsinchu, Taiwan, Republic of China

中 華 民 國 九 十 四 年 七 月

國 立 交 通 大 學

論文口試委員會審定書

本 校 光 電 工 程 研 究 所 碩 士 班 ___吳勝隆___ 君

所提論文 兆赫技術應用於豬皮燒傷深度的檢驗及血紅素光譜量測

合 於 碩 士 資 格 標 準 、 業 經 本 委 員 會 評 審 認 可 。

口試委員：

林恭如 教授　　　　　　　　趙如蘋 教授

孫啟光 教授

指導教授：

潘犀靈 教授

所　　長： _____ 教授

賴暎杰 教授

系 主 任： _____ 教授

潘犀靈 教授

中 華 民 國 九十四 年 七 月 二十七 日

中文摘要

兆赫時域光譜技術可應用於兆赫波段光譜的研究。此研究工作利用兆赫時域光譜技術獲得正常與燒燙傷豬皮的折射係數與吸收係數，在 0.6 兆赫的折射係數分別為 1.68 ± 0.01 與 1.76 ± 0.02，吸收係數則為 12.4cm^{-1} 與 10.8cm^{-1}。所有的豬皮樣品均經由丙酮溶液去除水分以減少水對兆赫波訊號的吸收。這個技術也用來觀察到燒傷豬皮雙折射特性減弱的情形。此外，兆赫時域光譜技術也用來獲得粉末狀以及薄膜狀血紅素在兆赫波段的光譜資訊，血紅素在 0.2 到 1.2 兆赫的範圍有寬頻的吸收，用這個方法得到粉末狀及薄膜狀血紅素在 0.1 兆赫的折射係數分別為 1.86 ± 0.01 與 1.61 ± 0.05，吸收係數則為 25cm^{-1} 與 30cm^{-1}。我們進一步應用兆赫光譜技術來作樣品反射式訊號的量測，可以觀察到用來模擬部分燒傷的皮膚的由一層燒燙傷以及一層正常的豬皮樣品堆疊成的結構中的界面，經由這個模擬結構表面以及內部界面和背面反射的訊號波形都可以正確清楚地判別，所得到反射的波形以及表面和界面間的飛行時間和個別量測正常及燒燙傷樣品的結果吻合。經由這些初步的實驗結果應用到真實燒燙傷深度的判斷將是有可能的。

i

Abstract

THz time domain spectroscopy (THz-TDS) is for spectroscopy studies in THz ranges. In this work, THz-TDS is applied to characterize refractive indices and absorption coefficients of normal and burned porcine skin of 1.68 ± 0.01 and 1.76 ± 0.02, 12.4cm^{-1} and 10.8cm^{-1} at 0.6THz, respectively. All of the skin samples are dehydrated with Acetone to reduce the water absorption in THz ranges. Birefringence reduction of burned porcine skin has also been observed by this technology. In addition, the spectroscopic information of powder and thin-film porcine hemoglobin in THz range is acquired. Hemoglobin has broadband absorption from 0.2THz to 1.2THz. The measured refractive indices and absorption coefficients of powder and thin-film hemoglobin are 1.86 ± 0.01 and 1.61 ± 0.05, 25cm^{-1} and 30cm^{-1} at 1THz. Further reflective type measurement can be implemented by THz-TDS. Interface information is obtained from the measured THz waveform reflected from stacked burned and normal porcine skins for simulating partial burned skin. Reflective wave from surface, interface between burned and unburned, back surface of unburned porcine had been correctively and clearly observed. Waveform and time of flight matched well with the original reflected waveform of normal and burned porcine skin. Clinical burned depth detection will be possible from these initial experiments.

Acknowledge

誌謝

　　鳳凰花開又謝，碩士班的生涯即將告一段落。如果是一年多前，可能沒想過今日的自己能夠踏在這個地方完成學業，要感謝的人實在太多了。

　　首先要感謝的是指導教授潘犀靈老師對於實驗及生活上悉心的教導與關心，讓我能在優良的研究環境中從容地進行研究工作。

　　接著是在實驗工作上耐心引領指導我的劉子安學長。學長專業的學術素養以及執行實驗細心嚴謹的精神還有為人處世的虛懷若谷，對我從事研究的態度有了很大正面的影響。謝謝學長！

　　感謝王怡超學長以及陳晉瑋學長在雷射系統方面的維護及調整，讓我有穩定的雷射光源進行實驗。

　　在實驗方面還要感謝工研院量測中心的周儒修先生，於生醫方面提供了很多協助及建議。

　　另外感謝羅誠在我剛踏入這個陌生環境時，不吝惜給予我這陌生人指導以及關心，以及常跟我分享實驗心得及生活上喜怒哀樂的小冷還有一起打拼論文的宗翰、仔仔、小壯、cc 和小高。此外謝謝學妹乃今的加入為我們帶來一股清新的活力，生活上也多了許多歡笑。

　　當初幸虧家任及時地拉了我一把，還有卓帆不斷地給予建議與鼓舞，使我得以能夠堅持到現在。兩位大學的換帖好兄弟，謝謝你們！

　　謝謝我的父母，無怨無悔辛勤地工作並給予我鼓勵支持，使我的研究過程可以無後顧之憂。

　　最後，僅以一首詩來抒發我的感想：

研究生活甘苦交雜
　　如人飲水各有牽掛
萬事若能始終堅持
　　雨過天晴自是豁達

風城遊子 勝隆
于 新竹交大
2005/07/28

Contents

List of Figures and Tables

1. Introduction

1.1 Introduction of Thermal Damage on Tissue Injury

Tissue injury due to thermal damage is very common in daily life. Estimates related to the annual incidence of burns in Taiwan is approaching two hound thousands cases in 2003 [1]. Traditionally, burns have been divided into first-, second-, third-, and fourth degree injuries, as shown in Fig. 1.1.

Average Depth < 0.735 mm

Average Depth of 0.735 – 2.535 mm

Average Depth of 2.535 –3.0 mm

Average Depth of 3.0 –30.0 mm

First Degree

Second Degree

Third Degree

Fourth Degree

Epidermis

Dermis

Deep dermis

Hypodermis

Muscle

Bone

http://www.cgmh.org.tw/intr/intr2/c32930/knowledge.htm#5
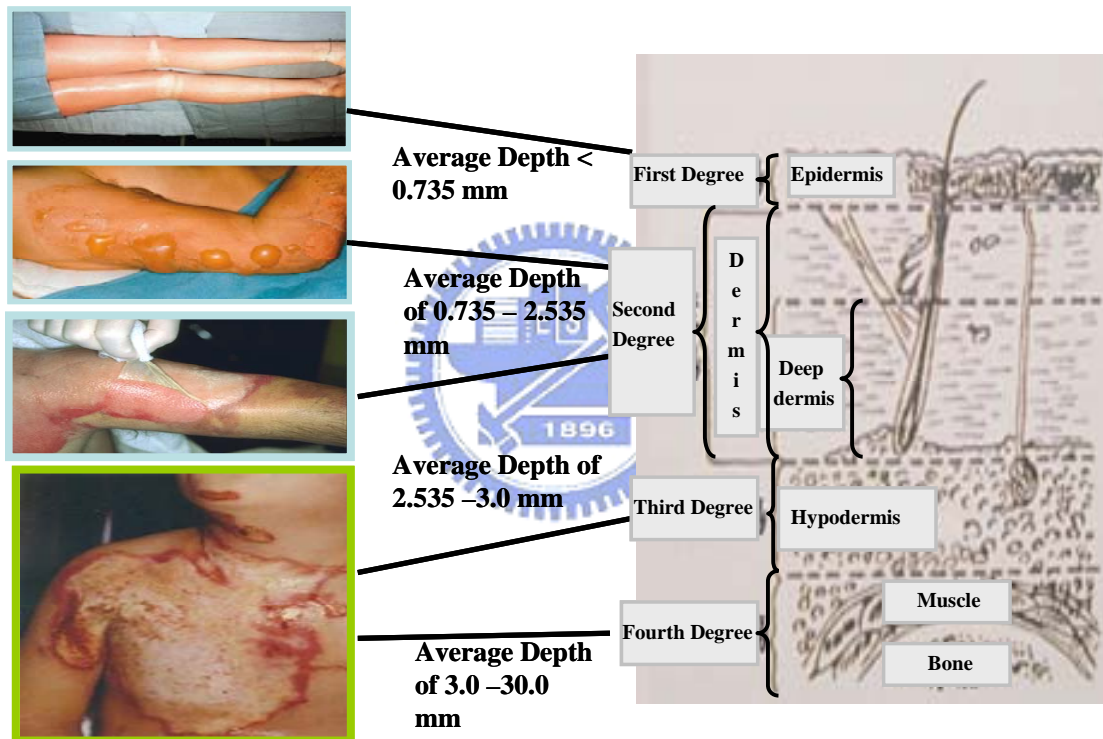
Fig. 1.1 Schematic of classification of burns

First degree burns, which are limited to epithelial damage (average depth < 0.735mm) [2], heal spontaneously and do not require treatment. Third or fourth degree burns, which are complete full thickness destruction of the epidermis and dermis (> 2.535mm), are treated with an autologous or transplanted skin graft. A second burns shows destruction

of the epidermis and partial destruction of the underlying dermis (0.735-2.535mm). If the injury produces a superficial partial thickness burn, then it is best to allow the wound to heal spontaneously from surviving skin appendages. Conversely, if the injury produces a deep partial thickness burn, then it would be wise to skin graft the wound as soon as possible to avoid infection.

Non-invasive determination of the depth of tissue injury due to thermal damage is very important. X-rays is a very common source for diagnosing diseases, while it is harmful for human bodies for its high photon energies in the range of keV. T-rays have several advantages over x-rays, one being that they have low photon energies (For example, 4meV at 1THz) and therefore do not subject a biological tissue to harmful radiation. While microwave and x-ray imaging modalities produce density pictures, T-ray imaging also provides spectroscopic information within the terahertz frequency range. The unique rotational, vibrational and translational responses of materials (molecular, radicals and ions) within the THz range provide information that is generally absent in optical, x-ray and NMR images. In principle, these transitions in THz frequency are specific to the molecule and therefore enable THz wave fingerprinting. This conformational information is closely related to biological functions of the molecules in tissues and cells and is difficult to access with other techniques [3].

Coherent THz wave signals are detected in the time domain by mapping the transient of the electric field in amplitude and phase. This gives access to absorption and dispersion spectroscopy. T-rays can also easily penetrate inside most dielectric materials, which may be opaque to

visible light and low contrast to x-rays, making T-rays a useful and complementary diagnostic source.

A conventional method to determine burn depth is polarization sensitive optical tomography (PSOCT) in the near infrared range [4] [5]. THz radiation was used to measure human skin tissue [6] and pork tissue [7], but the measurement of burned sample of porcine skin has not done to our knowledge.

1.2 Birefringence of Collagen in Biological Tissue

Collagen, a constituent of many biological tissues, is in rod-like triple helix conformation, which results in both linear and circular anisotropic properties [8] [9]. Thus, collagen is a linearly birefringent tissue constituent. The fundamental building block The fundamental building block of collagen fibers is the tropocollagen molecule. Tropocollagen is comprised of three left-handed α-helices that combine to form a single right-handed super helix. The collagen fiber is formed from a staggered array of the tropocollagen molecules. The molecular packing structure of a collagen fiber is such that the refractive index along a fiber's length is greater than the cross-sectional refractive index [9] [10] [11]. Thus native collagen type I has a uniaxial semicrystalline conformation, where the refractive index parallel to the length of a tendon is larger than the refractive index along any orthogonal axes in the plane of the tendon's crossection.

Yoshioka and O'Konski [9] reported the birefringence (Δn) is 1.2×10^{-6} for tropocollagen extracted from native rat tail tendon, in a

0.022g/L dilute solution of collagen in 0.0029 molar acetic acid. Naylor found a lamellae birefringence of $\Delta n = 3.0 \times 10^{-3}$ from in vitro cat cornea [11]. Stanworth and Naylor showed that bovine lamellae birefringence is 2.8×10^{-3}.

Upon heating, the transition by collagen from a α-helix, which can be viewed as rod-like, to a random-coil conformation is accompanied by a loss of birefringence. Research shows that birefringence of collagen is reduced by denaturation that takes place at a temperature between 56 -65 °C. The normal dermis is made up of irregular collagen fibers and fibroblasts having an orientation roughly parallel to the skin surface. Thermal injury will denature dermal collagen, resulting in a reduction of birefringence, thus providing an "optical marker" for thermal damage.

1.3 Formal Works of Spectroscopy of Hemoglobin

Mammalian hemoglobin (Hb) has molecular weights of about 64,500 [12]. Fig. 1.2 (a) shows the configuration of hemoglobin molecule. It is composed of four peptide chains called globins each of which is bound to a heme. The molecule of heme is shown in Fig. 1.2 (b).

Normal human hemoglobin is composed of a pair of two identical chains. Iron is coordinated to four pyrrole nitrogens of protoporphyrin IX. Hemoglobin responsible for the transport of oxygen from the lungs to tissue is primarily contained inside red blood cells (RBCs) and can reversibly bind up to four oxygen molecules to form oxygenated hemoglobin (HbO_2).

M. F. Perutz, *The Hemoglobin Molecule*
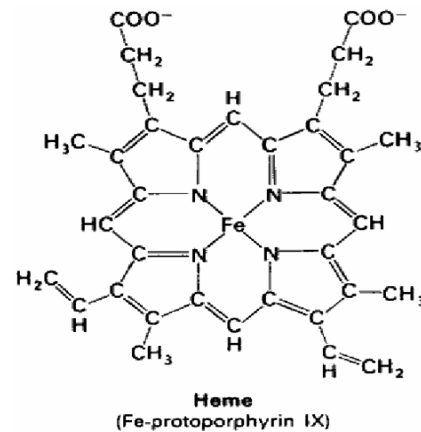
(a)   (b)

Fig. 1.2 (a) The mammalian hemoglobin molecule

(b) The heme molecule

Hemoglobin is very important for the biomedical researches, especially for the spectroscopy comparison among deoxyhemoglobin (deoxy-Hb), HbO_2 and HbCO. Hb in normal human blood is coordinated with dioxide. However, it will result in shock, stupor or dead if Hb is coordinated with carbon oxide. Many researches focused on frequency ranges from visible light (VIS) to near infrared (NIR). For example, refractive index of HbO_2 and Hb are around 1.395 with anomalous dispersion around 410nm, which represented the band edge absorption, as shown in Fig. 1.3 (a) [13]. Absorption spectrum among deoxy-Hb, HbO_2 and HbCO had also been performed [14]. As the content of oxygen increased, the band absorption peak around 410nm and double peak around 560nm and 540nm is blue shifted and more obviously with respectively in the VIS range. The obvious peak around 720nm in case of

deoxy-Hb, which is not observed in HbO_2 in the NIR range, can be used as the fingerprint spectroscopy for distinguishing these two materials [13]. However, spectroscopy of Hb in THz range is not yet available from our knowledge.

Dirk J. Faber et. al,
PHYSICAL REVIEW LETTERS, **93, 028102,**

T. K. Das et. Al. Biochemistry **2000,**
39, 14330-14340
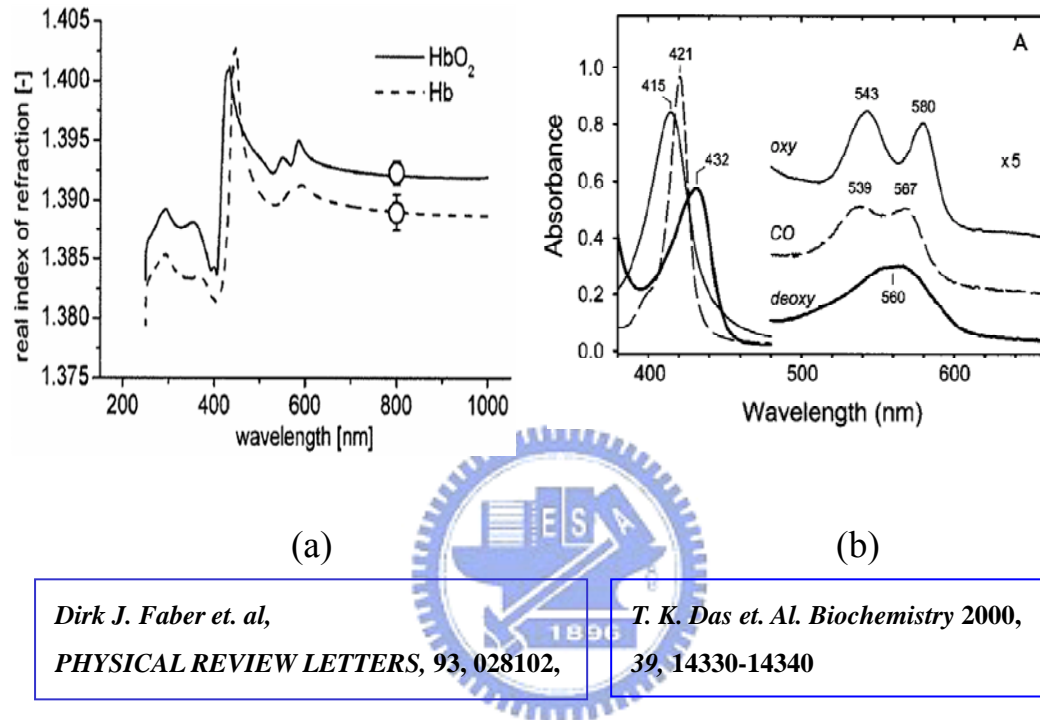
Fig. 1.3 (a) Refractive index of Hb and HbO_2 in VIS-NIR region

(b) Absorption coefficient of Hb, HbO_2 and HbCO in

VIS-NIR region

Blood spectrum around THz range had been demonstrated [15]. The absorption coefficient of Blood and water from 0.5THz to 1.5THz is gradually increased from $120cm^{-1}$ to $240cm^{-1}$ and $150cm^{-1}$ to $250cm^{-1}$, as shown in Fig. 1.4 (a), Fig. 1.4 (b), respectively. However, blood contained not only hemoglobin and water but also leukocyte and platelet. THz radiation is not only possible for transmitting skin with less scattering effect than NIR, but also can detect the blood spectrum directly.

(a)   (b)
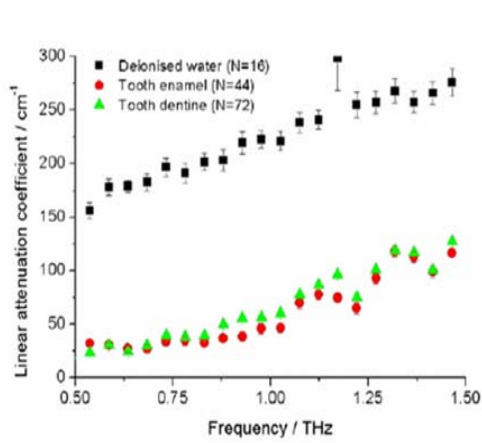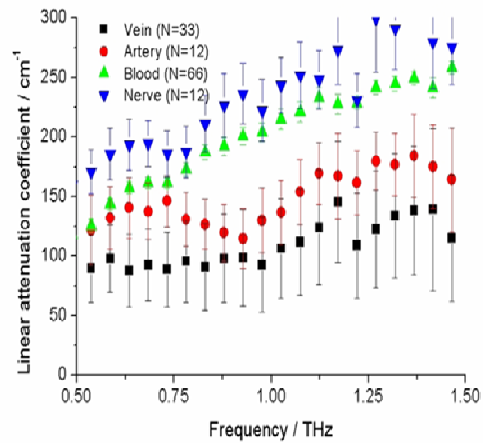
Fig. 1.4 (a) Absorption coefficient of blood etc. in THz range

(b) Absorption coefficient of water etc. in THz range

2. Principle

2.1 THz Time Domain Spectroscopy

Terahertz waves, with a frequency range of 0.1-10 THz, are termed 'T-rays'. They occupy a large portion of the electromagnetic spectrum between the infrared and microwave bands, as shown in Fig. 2.1 [16]. The large terahertz portion of the spectrum has not been well developed because there were neither convenient high-power convenient high-power emitters to send out controlled terahertz signals nor efficient sensors to collect them and record information until the development of THz time domain spectroscopy (THz-TDS).

A G Davis et al, Phys. Med. Biol. 47, 3679-3689
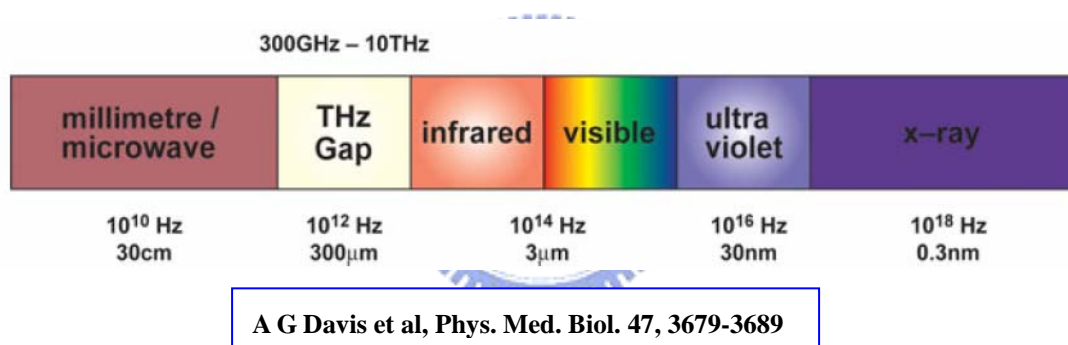
Fig. 2.1 A schematic representation of the electromagnetic spectrum showing the THz region

THz-TDS was initially developed in the early 1980s. Auston and Cheung used electro-optic materials to rectify fs optical pulses, thereby producing THz radiation of approximately one cycle. The coherence detection of the electric field of these THz pulses by electro-optic sampling enabled measurement of the changes in the shape of the waveform following reflection or transmission from materials. In this way the dielectric response of semiconductor materials was measured. A

THz-TDS comprises a femtosecond laser source, the output from which is split such that a part is used to produce THz radiation which passes through the sample using an electro-optic sampling system (or PC antenna detection system). Fig. 2.2 and Fig. 2.3 show the conventional THz-TDS EO sampling system and antenna detection system [17].
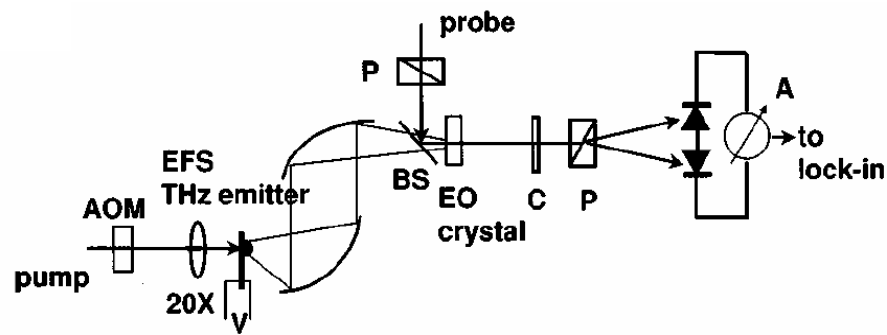
Y. Cai et al, Appl. Phys. Lett. 73, 1998

Fig. 2.2 Conventional THz-TDS EO sampling system
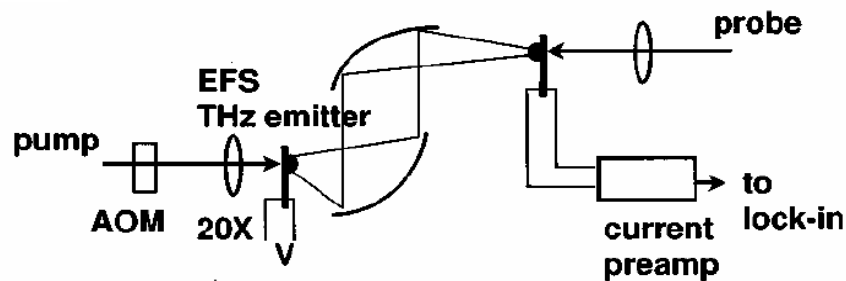
Y. Cai et al, Appl. Phys. Lett. 73, 1998

Fig. 2.3 Conventional THz-TDS PC antenna detection system

The THz TDS system provides a direct measurement of the THz electric field pulse E_{out} as a function of time t using a coherent time-gating pulse form the same laser as the pump pulse. If the sample has a transmission coefficient T, which is a function of frequency f, and produces a phase shift $\varphi(f)$ then the time-domain waveform in

9

transmission geometry can be derived from the incident THz spectrum $E_{in}(f)$ by

$$E_{out}(t) = \int_0^{\infty} E_{in}(f)T(f)e^{i\phi(f)}e^{2\pi ft}df \qquad (2.1)$$

2.2 Generation and Measurement Principle of THz Radiation

At frequencies up to approximately 0.5 THz, EM radiation may be generated by electronic devices, including resonant tunneling diodes, Gunn devices, field effect or bipolar transistors [18]. Another popular approach is to use lasers to generates short pulses (of duration less than 100 fs) of near infrared radiation (output wavelength of approximately 800nm) which are directed onto a non-linear optical crystal (such as ZnTe) or photo-conductive structure (such as photo conductive(PC) antenna).

Conventional detectors for THz radiation rely on bolometers cooled by liquid helium . These devices measure only the intensity of the radiation and do not provide any phase information. The sensitivity of these devices is also limited by background radiation. Thus a more common approach called free-space electro-optical sampling is developed by Wu and Zhang [19].

2.2.1 Generation of THz Radiation with PC antenna

When a femtosecond laser excites a biased semiconductor with photon energies greater than its bandgap (Fig. 2.4), electrons and holes are produced at the illumination point in the conduction and valence bands, respectively. An electromagnetic field radiating into free-space

with the help of an antenna is produced by the fast changes of the density of photocarriers and their acceleration due to the applied dc bias (V_b). The production of ultrashort currents with a full-width half-maximum (FWHM) of 1ps or less strongly depends on the carrier lifetime in the semiconductor [20].
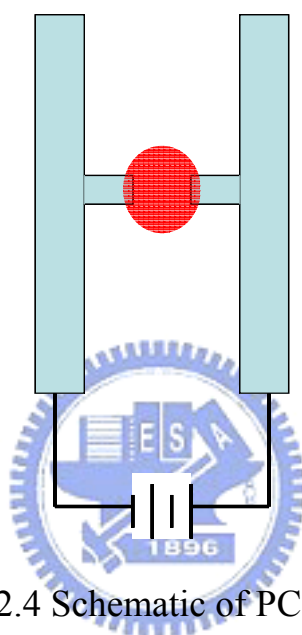
Fig. 2.4 Schematic of PC antenna

The carrier density behavior in time is given by

$$dn/dt = -n/\tau_t + G(t) \tag{2.2}$$

where n is the carrier density and $G(t) = n_0 \exp(t/\Delta t)^2$ is the generation rate of carriers due to laser pulse excitation, with Δt the laser pulse width and n_0 the generated carrier density at $t = 0$. The generated carriers are accelerated by the electric field bias with a velocity rate given by

$$dv_{e,h}/dt = -v_{e,h}/\tau_{rel} + (q_{e,h}E)/m_{eff,e,h} \tag{2.3}$$

where $v_{e,h}$ are the average velocity of the carrier, $q_{e,h}$ are the charge of the

electron and hole, τ_{rel} is the momentum relaxation time, and E is the local electric field, which is less than the applied bias E_b due to the screen effect of space charges. More precisely,

$$E = E_b - P/3\varepsilon_r \qquad (2.4)$$

where ε_r is the dielectric constant and $\boldsymbol{P}$ is the polarization induced by the separation of electrons and holes. The polarization depends on time according to the expression

$$dP/dt = -P/\tau_{rec} + J \qquad (2.5)$$

where τ_{rec} is the recombination time between electrons and holes (τ_{rec} = 10 ps for LT-GaAs) and $J = env_h + (-e)nv_e$ is the current density. The far-field radiation is given by

$$E_{THz} \propto \partial J/\partial t \propto ev\partial n/\partial t + en\partial v/\partial t \, , \qquad (2.6)$$

where $v = v_e - v_h$. The transient electromagnetic field E_{THz} consists of two terms: the first term describes the carrier density charge effect while the second term describes the effect of charge acceleration due to the electric field bias.

2.2.2 Measurement Principle of THz Radiation with EO Sampling

Fig. 2.5 is the schematic of EO sampling setup, which basically consists of an EO crystal, a quarter-wave plate, a Wollaston prism, and a balanced detector.

Electro-optic detection is a second-order nonlinear optical process in which an applied electric field induces a refractive index change in the EO crystal at visible-near IR frequencies that is proportional to the applied field. This refractive-index change affects the

ellipticity of a circularly polarized, synchronized, ultra short laser pulse that is co propagating through the same material. This change in ellipticity is measured with the Wollaston prism that separates the two orthogonal polarization components of the probe beam. The balanced detector measures the intensity difference between the two components and gives a signal that is directly proportional to the electric field. By varying the delay between the THz pulse and the probe-laser pulse, one obtains the complete time-dependent electric field.
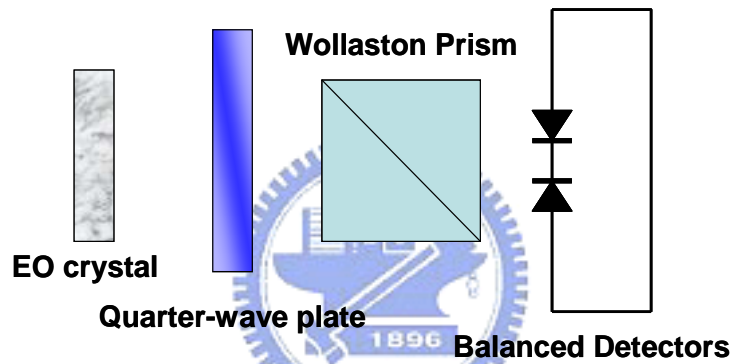

Fig. 2.5 EO sampling setup

The calculation of THz radiation is dependent on the refractive index ellipsoid that arises when an electric field is applied to the EO crystal. This index ellipsoid defines the refractive index in the crystal that is experienced by, for example, visible-near IR light propagating through the crystal with a given propagation direction and polarization. For a cubic crystal such as ZnTe, the only nonzero coefficient of the electro-optic tensor is r_{41}. If x, y, and z define the coordinate axes in the crystal [21], with the z axis corresponding to the (001) crystal axis, the refractive-index ellipsoid is given by

$$\frac{x^2}{n^2} + \frac{y^2}{n^2} + \frac{z^2}{n^2} + 2E_{THz,1}r_{41}yz + 2E_{THz,2}r_{41}xz + 2E_{THz,3}r_{41}xy = 1 \qquad (2.7)$$

where $E_{THz,1}$, $E_{THz,2}$, $E_{THz,3}$, are the components of the applied THz field E_{THz} along the x, y, and z direction, respectively. We assume the THz wave propagate along the (110) axis (shown in Fig. 2.4), thus $E_{THz,2}$=-$E_{THz,1}$.

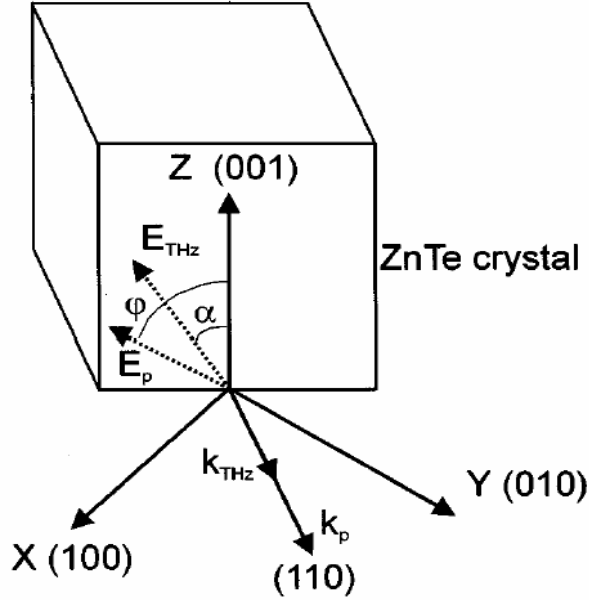After rotating the (x, y, z) coordinate system around the z axis by 45°, the equation (2.7) becomes:

Fig. 2.6 Angles of the THz wave and probe beam polarization directions

$$\frac{1}{n^2}(\frac{1}{2}\sqrt{2}x' - \frac{1}{2}\sqrt{2}y')^2 + \frac{1}{n^2}(\frac{1}{2}\sqrt{2}x' + \frac{1}{2}\sqrt{2}y')^2 + \frac{z'}{n^2} + 2E_{THz,1}r_{41}(\frac{1}{2}\sqrt{2}x' + \frac{1}{2}\sqrt{2}y')z'$$

$$+ 2E_{THz,2}r_{41}(\frac{1}{2}\sqrt{2}x' - \frac{1}{2}\sqrt{2}y')z' + 2E_{THz,3}r_{41}(\frac{1}{2}x'^2 - \frac{1}{2}y'^2) = 1$$

$$x'^2(\frac{1}{n^2} + E_{THz,3}r_{41}) + y'^2(\frac{1}{n^2} - E_{THz,3}r_{41}) + \frac{z'^2}{n^2} + 2\sqrt{2}E_{THz,1}r_{41}y'z' = 1 \qquad (2.8)$$

Than the (x', y', z') coordinate system is rotated around the x' axis

14

by θ :

$$x' = x''$$
$$y' = y'' \cos\theta - z'' \sin\theta$$
$$z' = y'' \sin\theta + z'' \cos\theta$$

The components of the electric field are expressed in terms of the angle α (the angle of the THz beam polarization with respect to the (001) axis shown in Fig. 2.6) :

$$E_{THz,3} = E_{THz} \cos\alpha$$

$$E_{THz,1} = E_{THz} \frac{\sqrt{2}}{2} \sin\alpha$$

With these definitions and some calculations, the index ellipsoid of (2.8) becomes :

$$x''^2 (\frac{1}{n^2} + E_{THz} r_{41} \cos\alpha) + y''^2 \{\frac{1}{n^2} - E_{THz} r_{41} [\cos\alpha \sin^2\theta + \cos(\alpha + 2\theta)]\}$$
$$+ z''^2 \{\frac{1}{n^2} - E_{THz} r_{41} [\cos\alpha \cos^2\theta - \cos(\alpha + 2\theta)]\} = 1$$

(2.9)

The refractive indices for visible-near IR light propagating along the x" direction are :

$$n_{y''}(\alpha) \approx n + \frac{n^3}{2} E_{THz} r_{41} [\cos\alpha \sin^2\theta + \cos(\alpha + 2\theta)]$$

(2.10)

$$n_{z''}(\alpha) \approx n + \frac{n^3}{2} E_{THz} r_{41} [\cos\alpha \cos^2\theta - \cos(\alpha + 2\theta)]$$

The intensity detected by balance detector can be expressed as :

$$\Delta I(\alpha, \varphi) = I_p \sin[2(\varphi - \theta)] \sin\{\frac{\omega}{c}[n_{y''}(\alpha) - n_{z''}(\alpha)]L\}$$
$$= I_p \frac{\omega n^3 E_{THz} r_{41} L}{2c} (\cos\alpha \sin 2\varphi + 2\sin\alpha \cos 2\varphi)$$

(2.11)

where φ is the angle of the probe beam polarization with respect to the (001) axis shown in Fig. 2.6.

15

2.3 **Calculated Method of Optical Constant from THz-TDS**

As shown in Fig. 2.7, the sample is taken as a multi-reflection structure for THz pulse [22]. The THz pulse before and after the sample insertion are denoted as $E_{ref}(t)$ and $E_{sam}(t)$, and their Fourier transforms are $E_{ref}^*(\omega)$ and $E_{sam}^*(\omega)$. If $E_{ref}^*(\omega)$ can be expressed as follows:

$$E_{ref}^* = E_0 e^{-ikd} \tag{2.12}$$

then the first, second and mth transmitted THz pulse $E_1^*(\omega)$, $E_2^*(\omega)$, and $E_m^*(\omega)$ are:

$$E_1^* = E_0 e^{-in^*kd}$$

$$E_2^* = E_0 e^{-i3n^*kd}(r_{sa}^*)^2 t_{as}^* t_{sa}^* \tag{2.13}$$

$$E_m^* = E_0 e^{-i(2m-1)n^*kd}(r_{sa}^*)^{2m} t_{as}^* t_{sa}^*$$

where n^* is the complex refractive index of the sample, t_{as}^*, t_{sa}^*, and r_{sa}^* are the real Fresnel coefficients for amplitude transmission and reflection at sample surfaces. n^*, t_{as}^*, t_{sa}^*, and r_{sa}^* can be expressed as follows:

$$n^* = n - i\kappa \tag{2.14}$$

$$t_{as}^* = \frac{2}{n^* + 1} \tag{2.15}$$

$$t_{sa}^* = \frac{2n^*}{n^* + 1} \tag{2.16}$$

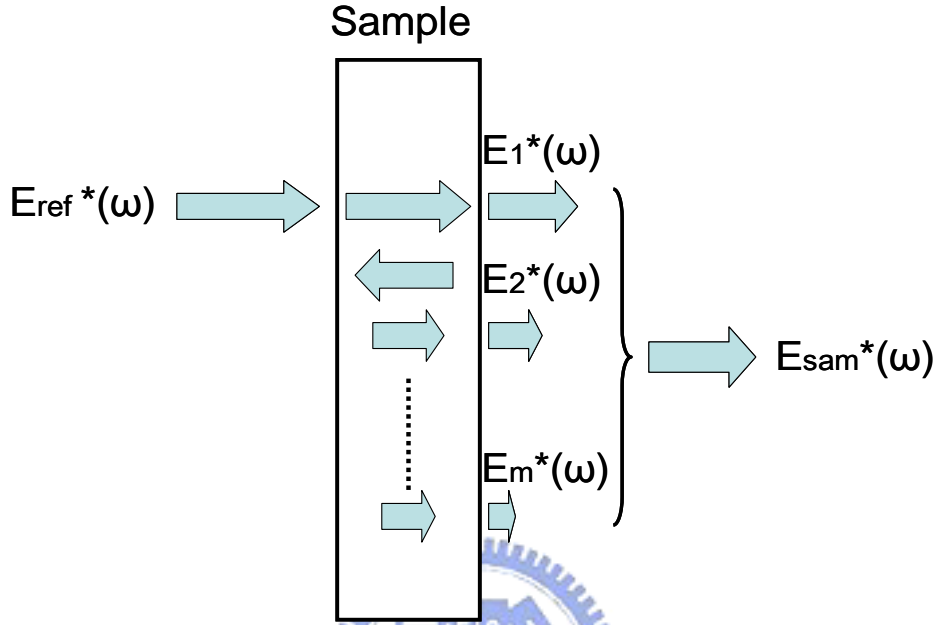$$r_{sa}^{*} = \frac{n^{*} - 1}{n^{*} + 1} \qquad\qquad (2.17)$$

Fig. 2.7 Schematic of multi-reflection structure of sample

Thus $E_{sam}^{*}(\omega)$ is the superposition all the transmitted electric fields.
The ratio of $E_{sam}^{*}(\omega)$ and $E_{ref}^{*}(\omega)$ can be given by n^{*} as:

$$\frac{E_{sam}^{*}(\omega)}{E_{ref}^{*}(\omega)} = t_{as}^{*} t_{sa}^{*} \exp\left(i \frac{(n^{*}-1)\omega d}{c} \right)$$

$$\times \sum_{l=0}^{m} \left(\left(r_{sa}^{*} \right)^{2} \exp\left(i \frac{2n^{*}\omega d}{c} \right) \right)^{l} \qquad (2.18)$$

$$\equiv \sqrt{T(\omega)} \exp(i\phi(\omega))$$

where d is the thickness of the sample, $T(\omega)$ and $\varphi(\omega)$ are experimentally obtained power transmittance and relative phase. Since it is difficult to obtain the complex refractive index n^{*} from

17

(2.18), the expressions for the real and imaginary parts of the complex refractive index of the sample are denoted as:

$$n = \frac{c}{d\omega}\left(\phi(\omega)+\frac{d\omega}{c}+\arg\left(t_{as}{}^{*}t_{sa}{}^{*}\sum_{l=0}^{m+1}\left(\left(r_{sa}{}^{*}\right)^{2}\exp\left(-i\frac{2n^{*}d\omega}{c}\right)\right)^{2}\right)\right)$$

$$\kappa = -\frac{c}{2d\omega}\ln\left(\frac{T(\omega)}{\left|t_{as}{}^{*}t_{sa}{}^{*}\sum_{l=0}^{m+1}\left(\left(r_{sa}{}^{*}\right)^{2}\exp\left(-i\frac{2n^{*}d\omega}{c}\right)\right)^{2}\right|}\right) \qquad (2.19)$$
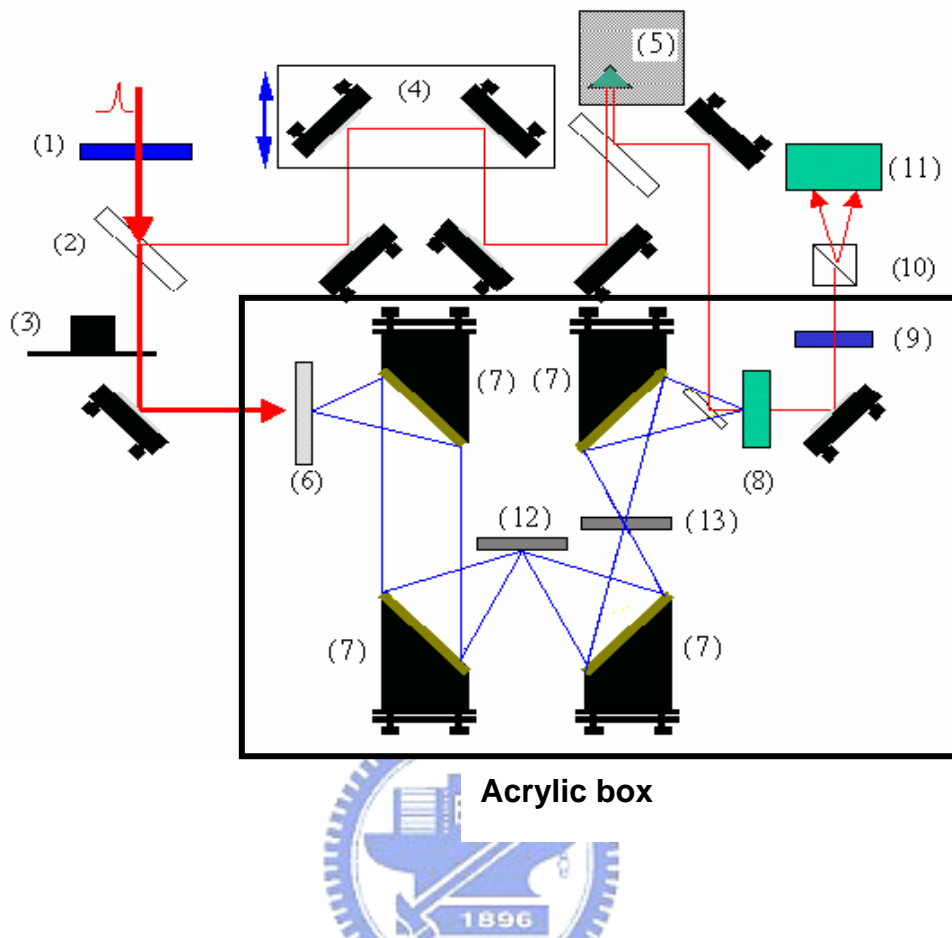
The value of the complex refractive index roughly estimated from the THz pulse in the time domain before and after the sample insertion is taken as a starting point for an iterative loop wherein n and κ are calculated in a self-consistent manner. By performing this cyclic procedure for only a few times, the value would lead to a convergence.

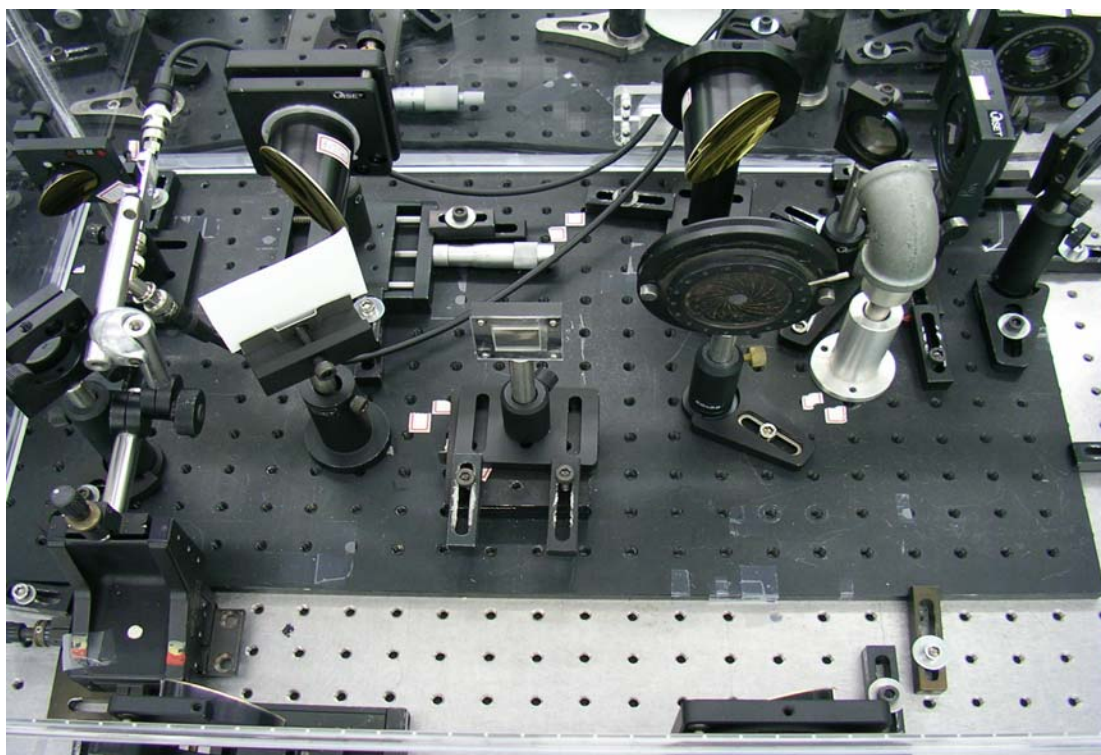# 1   Experimental Setup and Sample Preparation

3.1 Experimental Setup

The THz-TDS system is shown in Fig. 3.1(schematic) and Fig. 3.2 (real picture). Femtosecond pulses generated from a mode-locked Ti: sapphire laser are divided into pump and probe beams by a beam splitter (2). The pump beam is impinging on the THz emitter (6), dipole antenna on a GaAs: As$^+$ substrate to generate the transient current. Emission of electromagnetic pulses, THz radiation, with about picosecond duration is produced by the current. The THz radiation is collected and focused on a high reflection mirror (12) by the gold-coated parabolic mirrors (7) before passing through the sample (13) in reflected signal measurement.(In reflected signal measurement, the high reflection mirror is substituted with the sample). The probe beam with time delayed by motor stage (5) and the THz pulse collinearly impinged on a nonlinear crystal (ZnTe) (8). The transmitted laser pulse with polarization changed by electro-optical effect is separated into two beams with orthogonal polarizations by Wollaston beam splitter (10). The two beams are coupled to a balanced detector (11) connecting to a lock-in amplifier. Signal from lock-in amplifier can be easily analyzed by a computer.

To reduce the water vapor absorption of THz signal, an acrylic box by continuously infusing pure nitrogen is set as a humidity controller in THz optics. The humidity can be rapidly lowered to few percents in tens of minutes. Furthermore, due to the stable atmosphere in THz optics, the THz system becomes more stable.

Acrylic box

1. λ/2 plate
2. beam splitter
3. chopper
4. translation stage
5. optical delay stage
6. THz emitter
7. parabolic mirrors
8. ZnTe

9. λ/4 plate
10. Wollaston prism
11. balance detector
12. high reflection mirror or sample
    position of reflected signal
    measurement
13. sample position of transmitted
    signal measurement or nothing
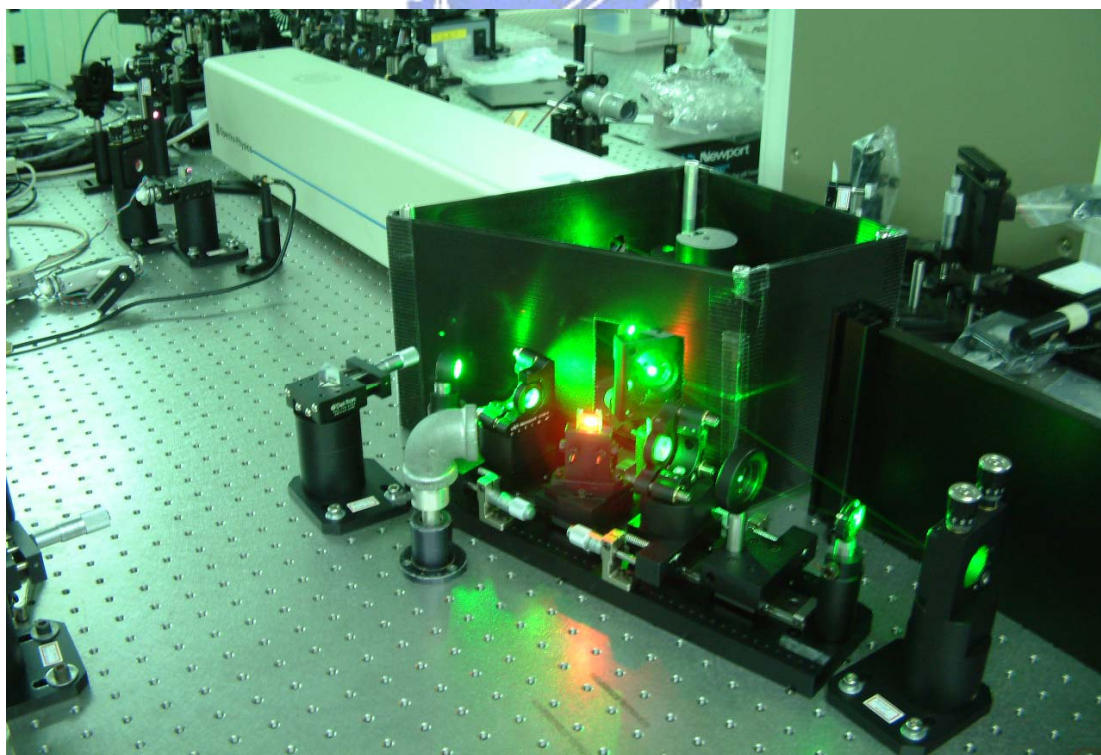
Fig. 3.1 Schematic of THz-TDS system

(a)

Fig. 3.2 Real pictures of (a) THz-TDS system and

(b) Ti-sapphire ultrafast laser

3.2 Sample Preparation

3.2.1 Preparation of Porcine Skin

The samples of porcine skins in the experiments are taken from streaky pork.

The thermal damage of burned porcine skins are formed by contacting normal skin using brass rod attached on welding machine or illuminating normal skin using cw laser.

The brass rod heating setup is shown in Fig. 3.3. Before contacting the porcine skin, the brass rod is preheated for 10 minutes with the welding machine to make sure the heat is uniformly transmitted in the brass rod. This method is a direct way to form the burned area, and it gives the temperature information of the thermal source.

Fig. 3.3 The heating brass rod and welding machine

Another method to form the thermal damage is to let porcine skin be illuminated by the laser beam. The beam size of the laser is not large enough to generate large area burns, which is needed in the measurement, thus the beam need to be broadened before illuminating on the skin. Fig. 3.4 is the schematic of the simple setup to broaden the laser beam and heat samples. The total measured power of laser beam illuminated on the sample is about 3.3 watt, and the illuminated process is not terminated until the back of the porcine been burned. The burned area is about 15mm in diameter.
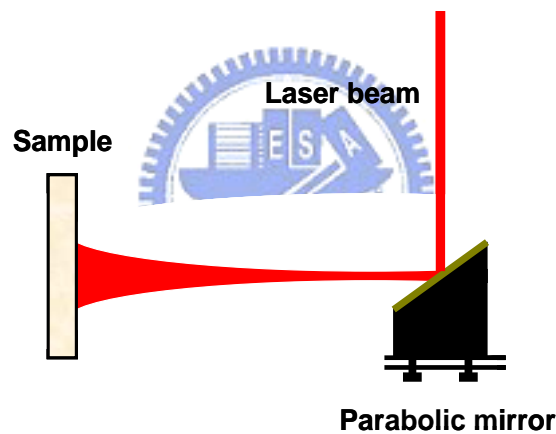

Fig. 3.4 Schematic of setup to broaden laser beam and heat samples

As a result of water has quite large absorption coefficient in the THz range (about 200cm^{-1} at 1THz) [23], all the samples need to be dehydrated to before measurement. All the porcine skins are dehydrated with Acetone solution. The porcine skins are clipped by glass to maintain the flatness of sample surface as immersing in Acetone solution for about 2 days.

3.2.2 Preparation of Hemoglobin

     The porcine hemoglobin samples are bought from UNI-WARD Corp. Two kinds of appearances of hemoglobin samples are made, as shown in Table 3.1.

	I	II	III
Type	**Powder**	**Powder**	**Thin film**
Thickness	**320±10µm**	**960±10µm**	**350 µm±50µm**

Table 3.1 Two kinds of hemoglobin samples

     Sample Type I and sample Type II are powders of hemoglobin of different thickness: 320µm and 960µm (thickness uncertainty ~ 10µm). This kind of appearance is applied to get the pure spectra of hemoglobin. Sample Type III is thin-film hemoglobin of thickness about 350µm (thickness uncertainty ~ 50µm). The thin-film of hemoglobin, which is used to model the under skin blood, is the product made by evaporating hemoglobin solution.

4. Experimental Results

4.1 THz waveform and spectrum

The measured THz waveform as the reference signal is shown in Fig. 4.1. The nitrogen is continuously infusing to THz-TDS system to reduce water vapor absorption of THz radiation. Fig. 4.2 is the spectrum of the measured THz radiation. The signal to noise ratio(S/N ratio) is about 10^6, and the absorption lines of water vapor at 0.557, 0.752, 0.988, 1.097, 1.113, 1.163, 1.208, 1.229 and 1.411 THz are not existed.
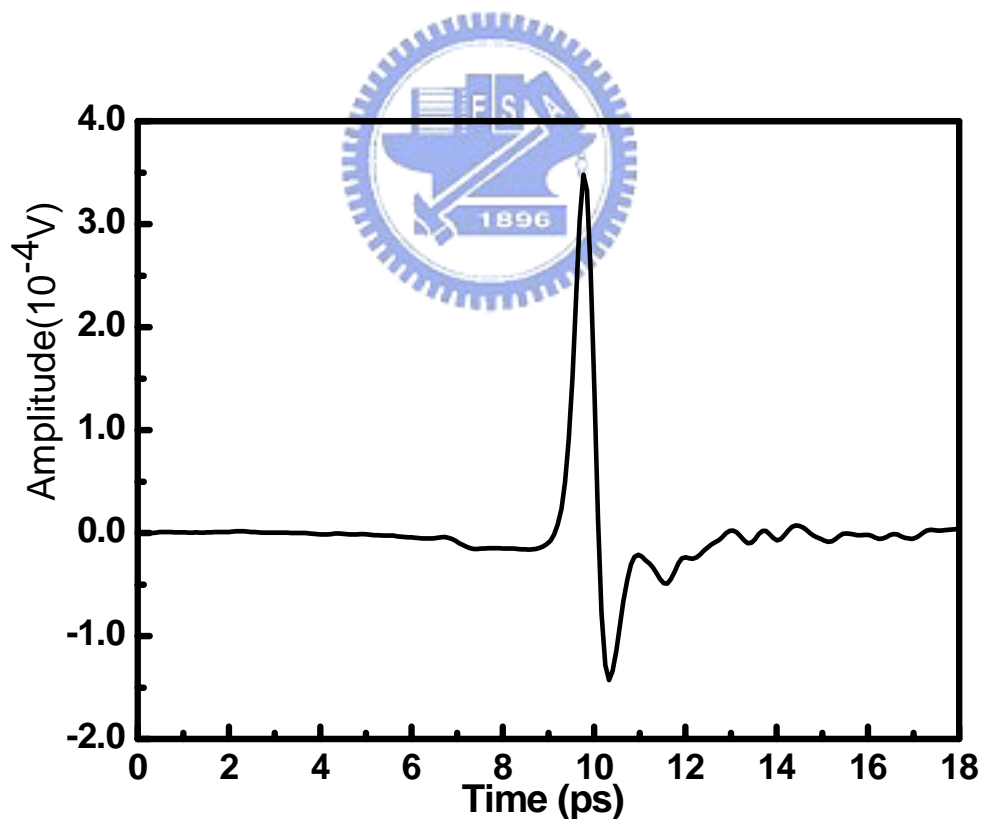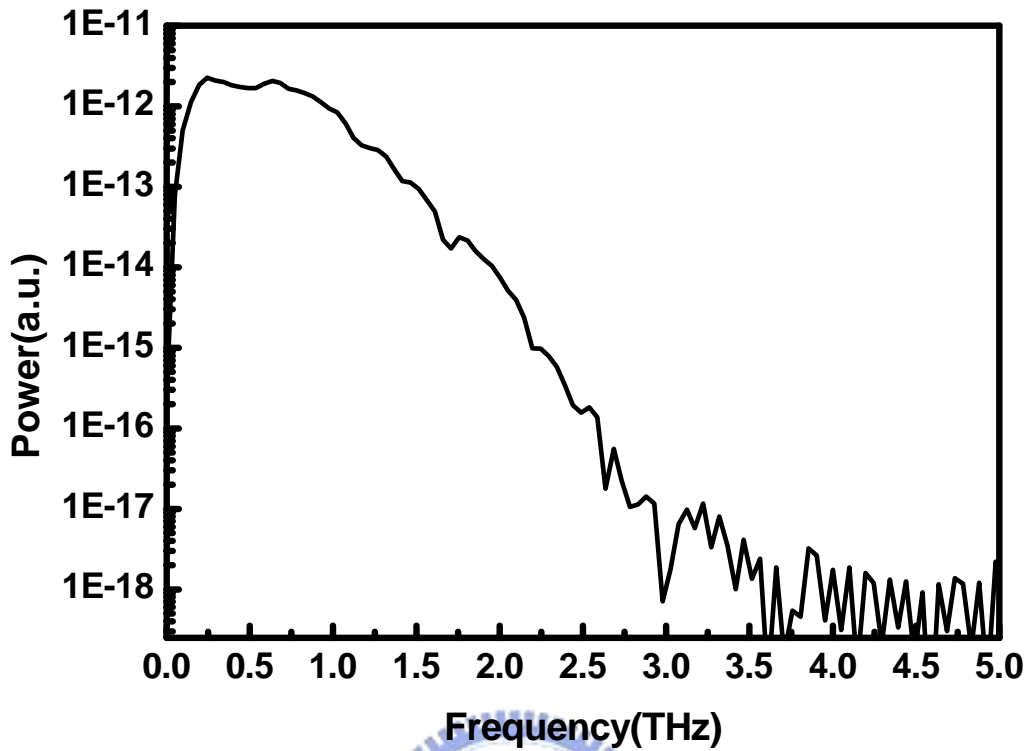

Fig. 4.1 Waveform of THz radiation

Fig. 4.2 Spectrum of THz radiation

4.2 Characterization Difference between Normal and Burned Porcine Skin

The preparation process and thickness of samples are shown in Table 4.1.

Type	Normal Porcine Skin	Burned Porcine Skin
Preparation process	Dehydrated with Acetone	1.Heated with brass rod attached on welding machine (130° C for 30secs) 2.Dehydrated with Acetone
Thickness	1.03±0.02mm	1.13±0.03mm

Table 4.1 Preparation process and thickness of samples

Fig. 4.3 shows the THz waveform of the reference signal and measured signals after passing through the samples (normal and burned porcine skin). From the time of flight of THz waveform, the refractive indices can be roughly calculated. The refractive index of normal porcine skin is about 1.65±0.01, while the burned porcine skin is about 1.74±0.02. Burned porcine skin has larger refractive index than normal porcine skin.

Fig. 4.4 represents the Fast Fourier transform (FFT) spectrum of the measured waveform in Fig. 4.3. In comparison with the reference spectrum, there are broadband absorptions for both normal porcine skin and burned porcine skin.

The transmittance (spectrum of sample divided by spectrum of reference) of THz radiation through porcine skins is shown in Fig. 4.5. From 0.2THz to 1.0THz, the transmittance decreases as the frequency increases for normal and burned porcine skins.

The refractive indices and absorption coefficients of porcine skins are shown in Fig. 4.6 and Fig. 4.7. In Fig. 4.6, the refractive index of normal porcine skin is from 1.77±0.01 to 1.66±0.01, which is smaller than the refractive index of burned porcine skin form 1.81±0.02 to 1.70±0.02 from 0.2THz to 1.0THz. In Fig. 4.7, the absorption coefficients of normal porcine skin and burned porcine skin is 1.5cm^{-1} to 24.2cm^{-1} and 0.1cm^{-1} to 30.2cm^{-1} from 0.2THz to 1.0THz individually. The uncertainties of refractive indices are calculated from the uncertainty of thickness. The change of absorption coefficients does not as obvious as refractive indices as the porcine skin is burned. The variation of refractive index can be a feature to differentiate burned porcine skin from unburned
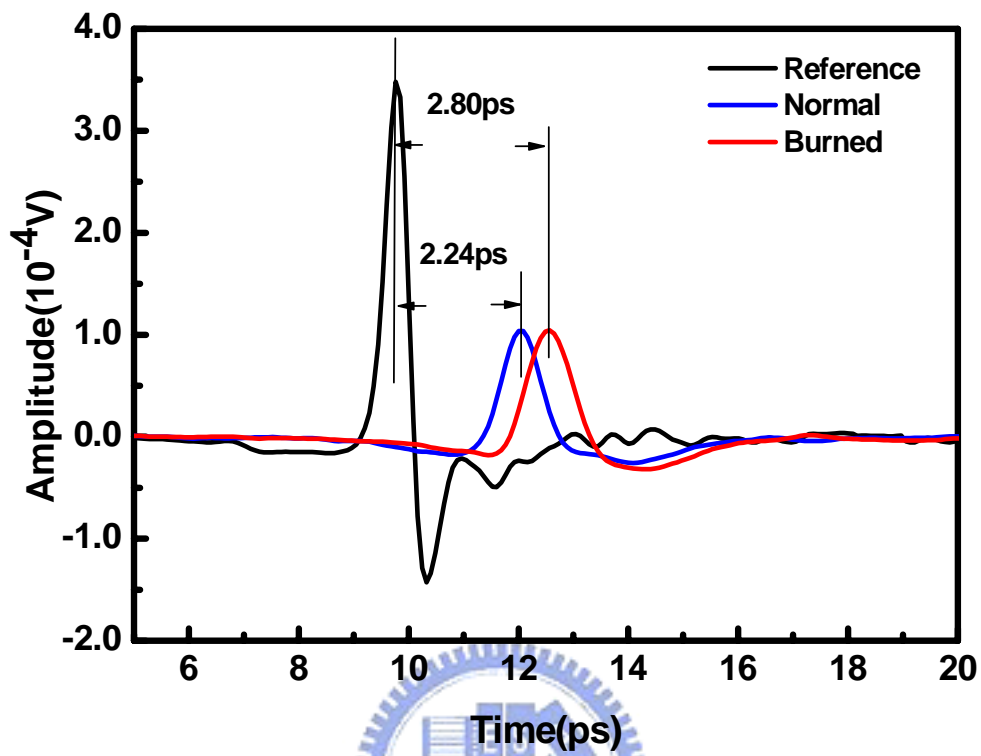
porcine.

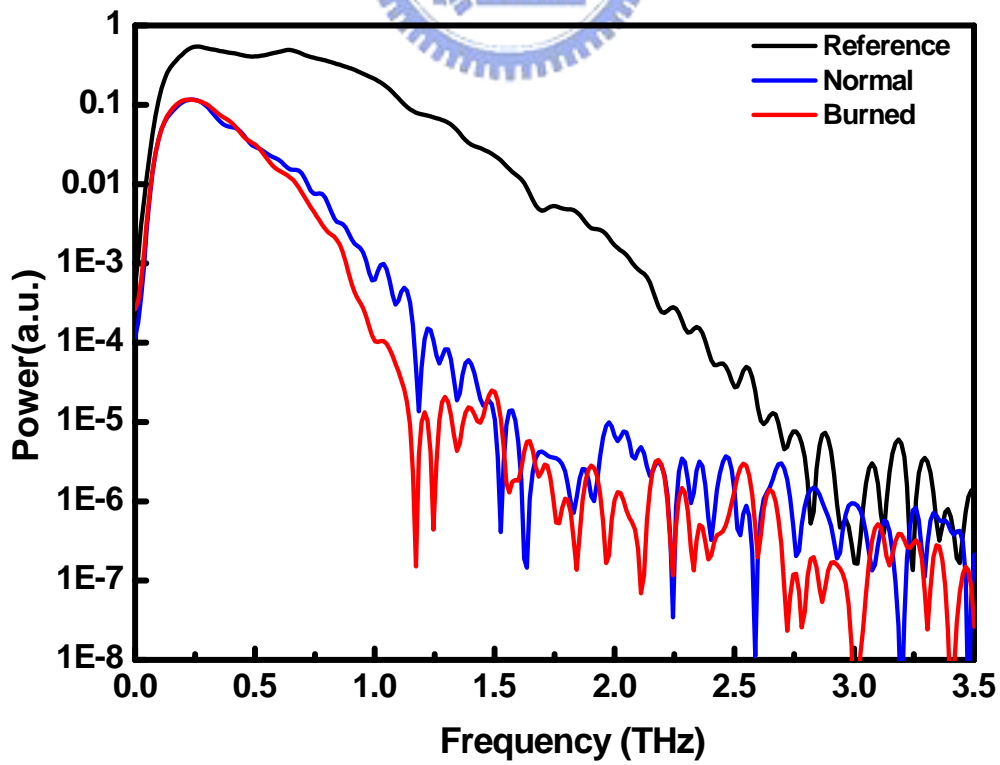Fig. 4.3 Waveform of transmitted THz signal
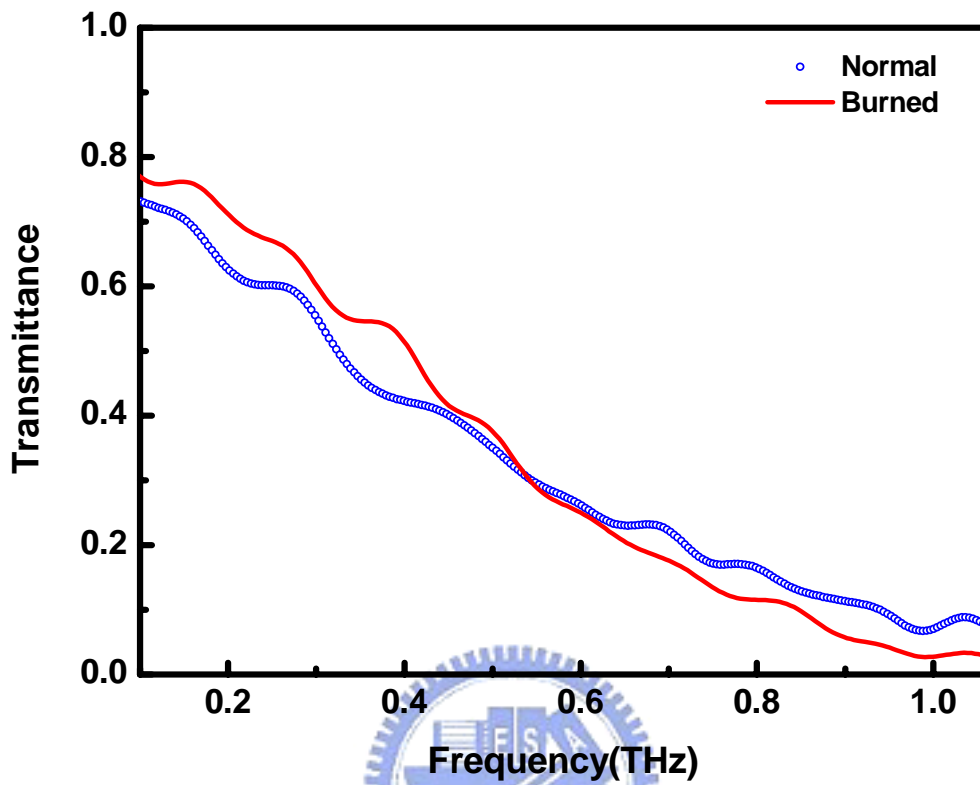

Fig. 4.4 Spectrum of transmitted THz signal
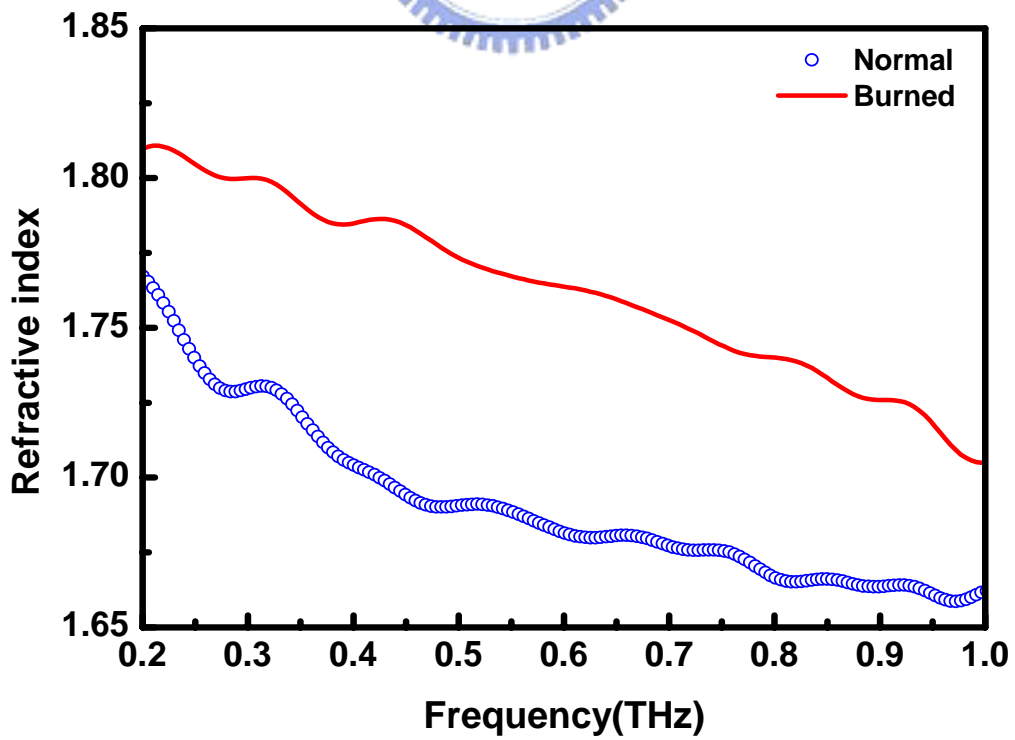
Fig. 4.5 Transmittance of THz signal through porcine skins

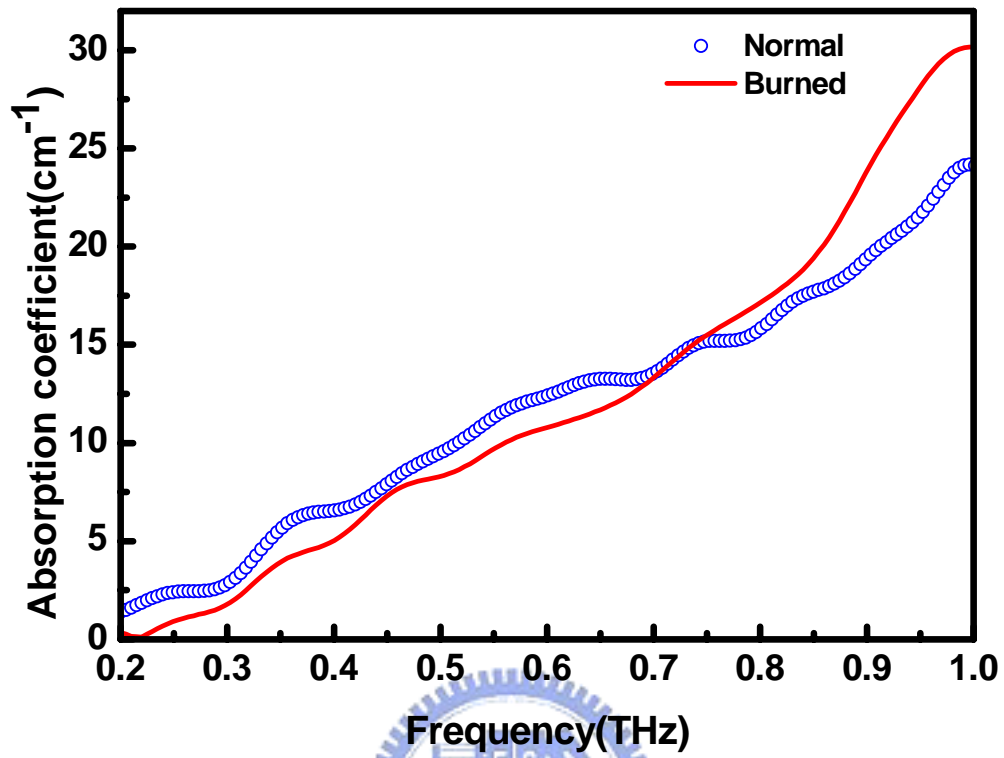Fig. 4.6 Refractive index of porcine skin from 0.2 THz to 1.0 THz

Fig. 4.7 Absorption coefficient of porcine skin from 0.2 THz to 1.0 THz

4.3 Denature of Birefringence of Burned Porcine Skin

The burned sample is made using cw lasers in the lab. Diameter of the burned area on the sample is about 15mm, with a measured power about 3.3 watts. The illuminated time is about 6 minutes.

Fig. 4.8 is the schematic of measurement mechanism. The sample rotates around the rotating axis shown in Fig. 4.6 to a certain angle θ for each measurement from 0° to 360°. THz radiation is measured after passing through the sample.
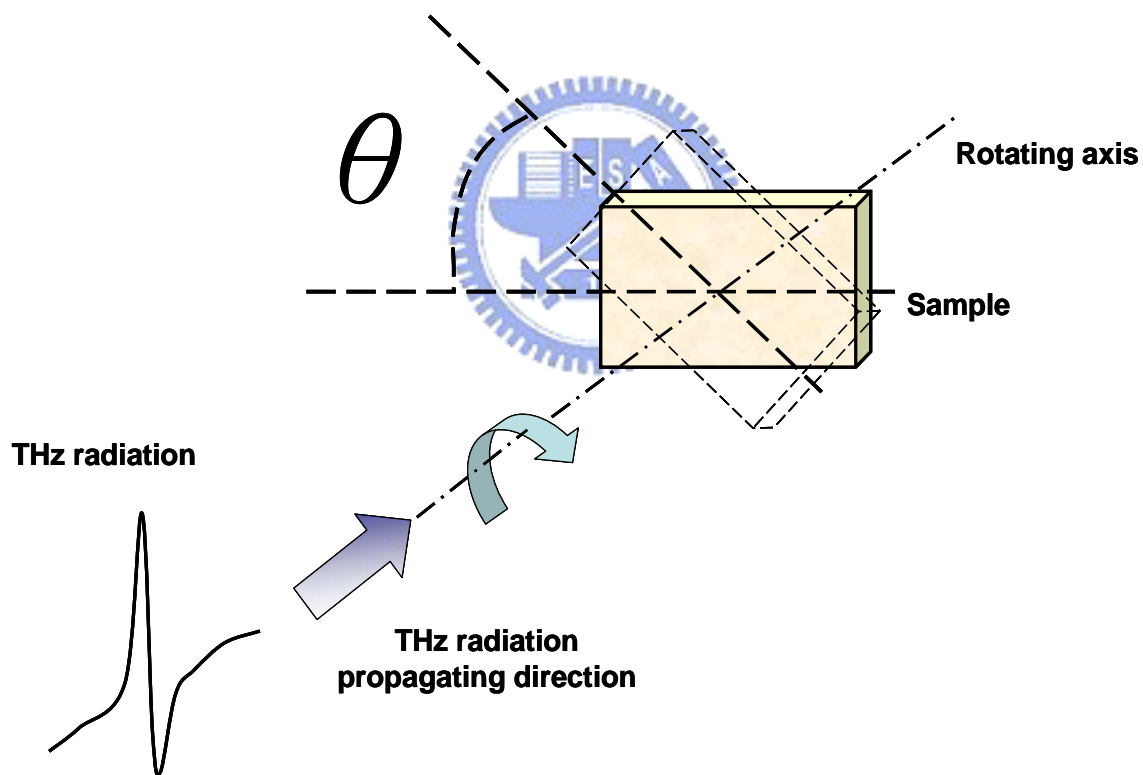

Fig. 4.8 Schematic of birefringence measurement

The transmitted THz radiation of normal porcine skin (thickness~1mm) is measured. Fig. 4.9 shows the measured waveform of
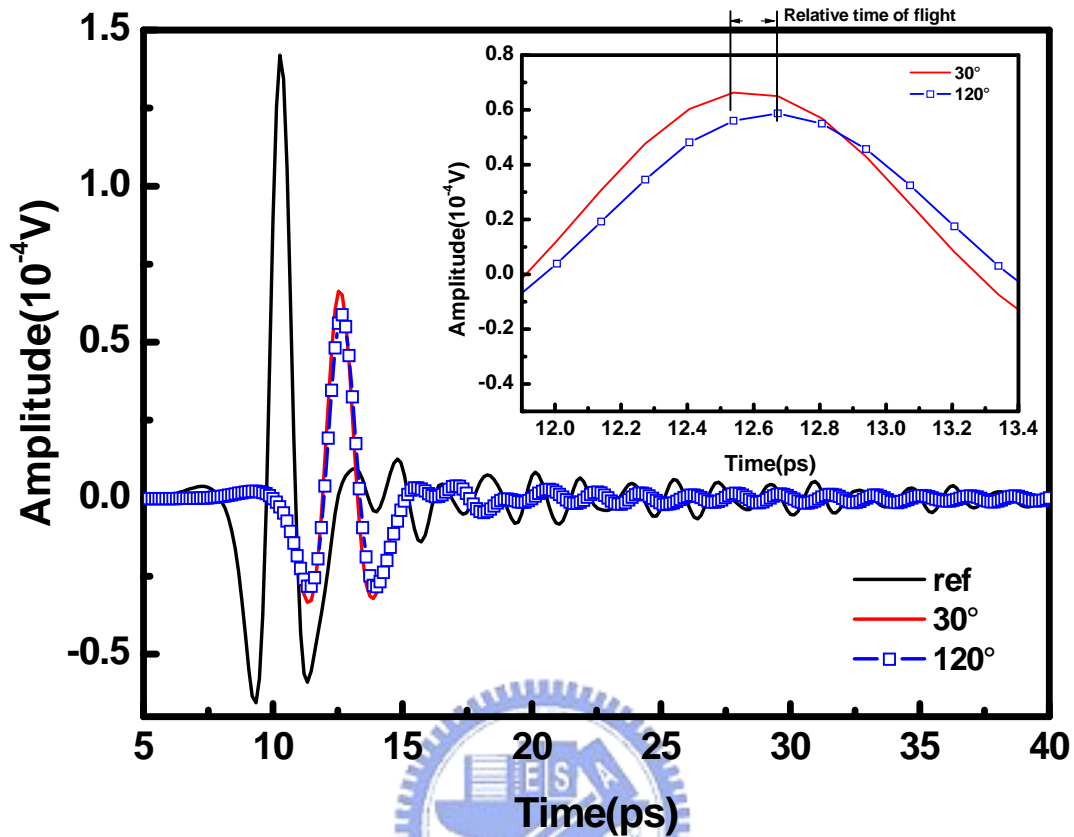
THz radiation.

Fig. 4.9 Measured waveform of THz radiation of normal porcine skin

In Fig. 4.9 only one THz pulse is observed in the full waveform. Inasmuch as the birefringence of collagen molecules in the dermis is weak ($\Delta n \sim 2.8 \times 10^{-3}$ of bovine lamellae) refer to former works [24], time of flight caused by the birefringence (Δn times sample thickness and divided by light velocity) is only about several one thousandth picoseconds, which is rather small in comparison with the FWHM (several picoseconds) of THz pulse. As a result, the measured waveform is the superposition of e-wave and p-wave.

As shown in Fig. 4.10, the data of time of flight have a periodic distribution for various angles. The angle difference from peak to peak of time of flight is about 90°, which is able to explain that the birefringence

exists in the normal porcine skin, since the included angle between fast and slow axis of a birefringence material is 90°.

Fig. 4.11 is the measuring results of relative time of flight versus angles of burned porcine skin. The data here are not as regularly as those of normal porcine skin, but there is still a little periodic distribution.

Fig. 4.12 and Fig. 4.13 demonstrate the refractive indices of normal porcine skin and burned porcine skin from 0.2 THz to 0.8 THz. In Fig. 4.12, the larger and smaller refractive indices correspond with the maximum and minimum time of flight shown in Fig. 4.10. Again it verifies the existence of birefringence of normal porcine skin. In Fig. 4.13, the distribution of refractive indices is more disorderly than those in Fig. 4.12. The birefringence of porcine skin denatures after suffering heating process, but there is still a little discrepancy of refractive index between two orthogonal angles.
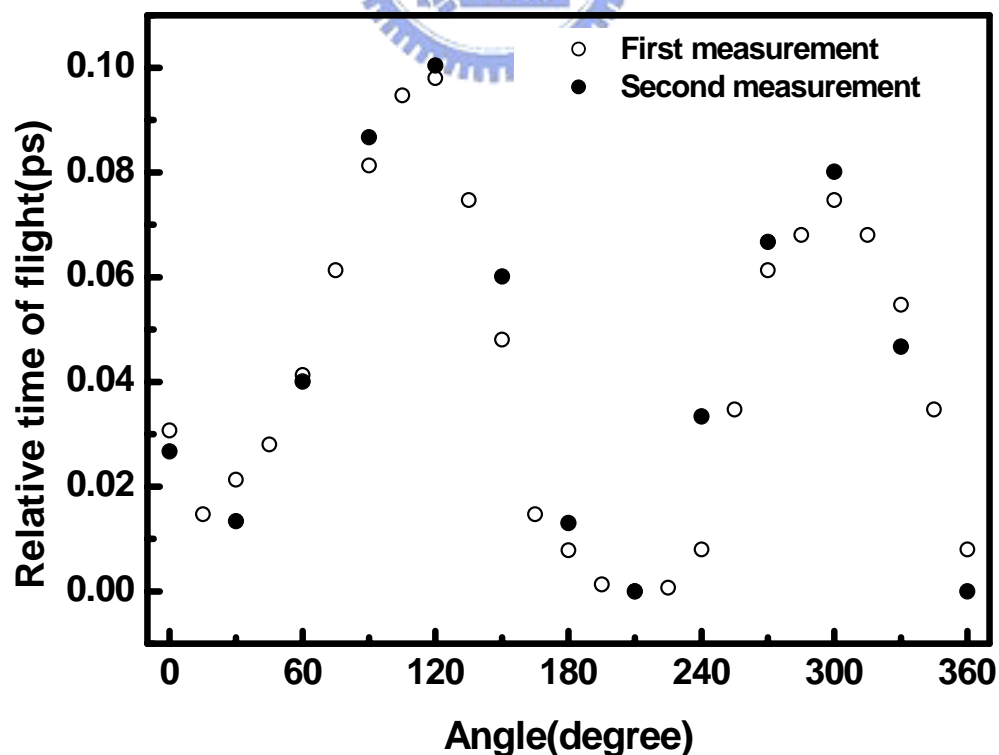

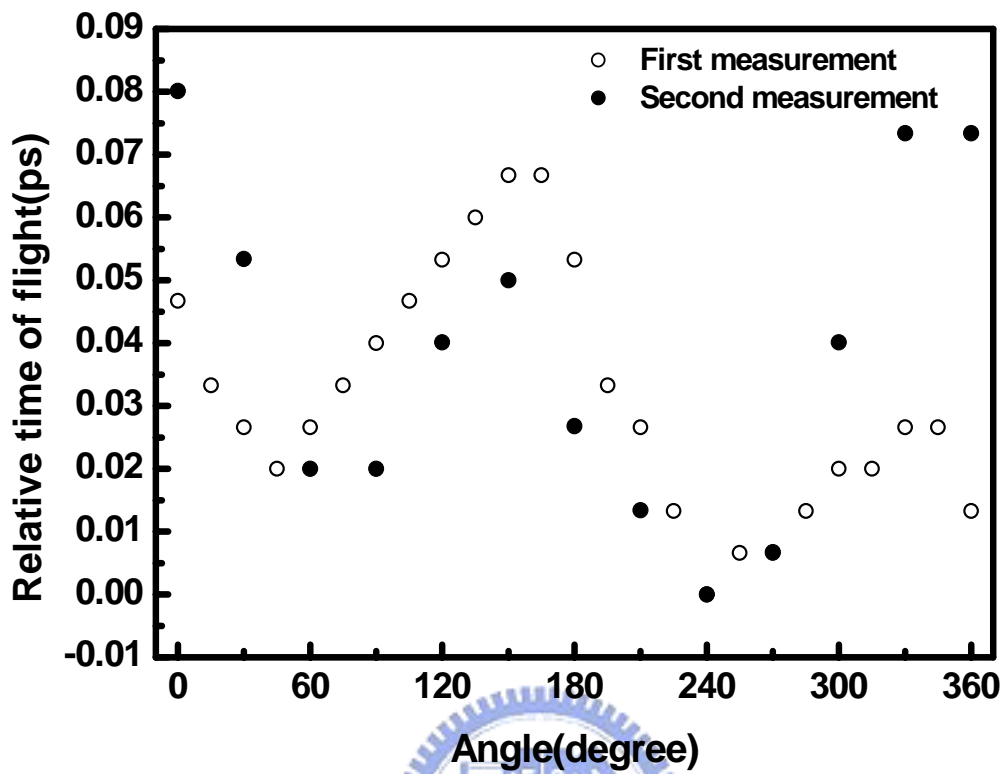Fig. 4.10 Relative time of flight of various angles of normal porcine skin

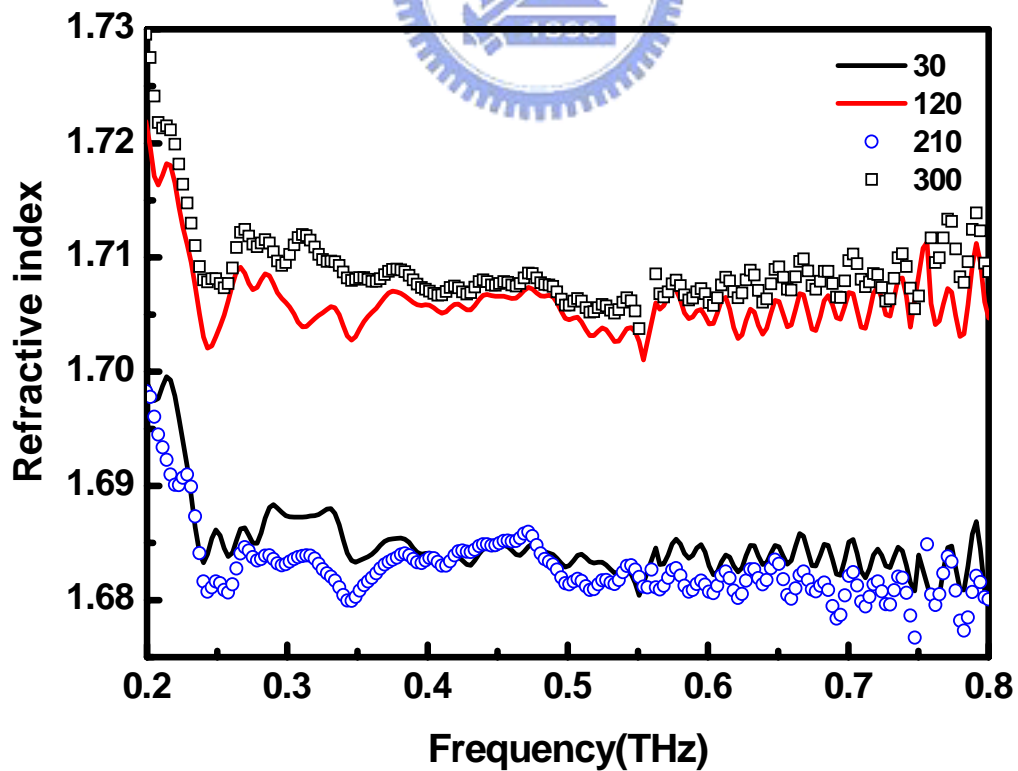Fig. 4.11 Relative time of flight of various angles of burned porcine skin

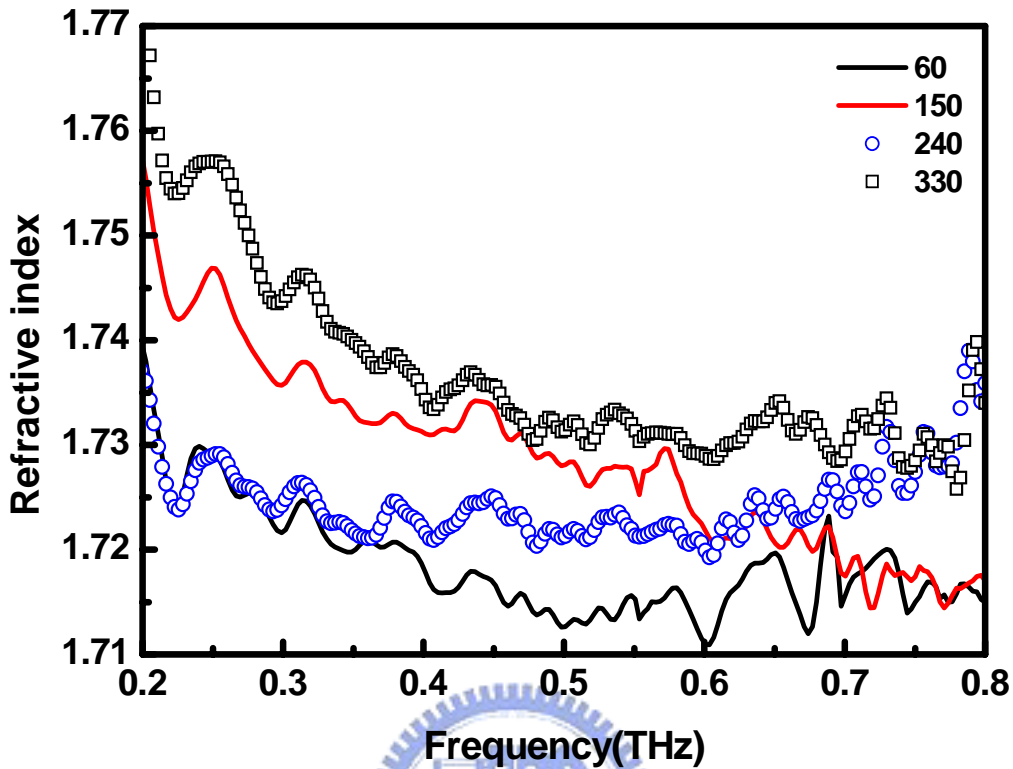Fig 4.12 Refractive index of normal porcine skin

Fig 4.13 Refractive index of burned porcine skin

There is a little difference of relative time of flight at 0° and 360° (represents the same included angle between sample and polarization of incident light) in Fig. 4.10. This phenomenon may cause form disturbance of the experimental setup. Fig 4.14 shows the maximum disturbances of reference signals by measuring the reference signals repeatedly. The maximum disturbance of time of flight is about 0.027ps. As a result, several normal porcine skins are stacked to get a thicker sample (thickness~11.53±0.2mm) to check the existence of birefringence. The measured result is shown in Fig. 4.15. The angle difference from peak to peak of time of flight is still 90°, and effect of disturbance (0.02ps) is quite small in comparison with the maximum time of flight (0.6404ps).
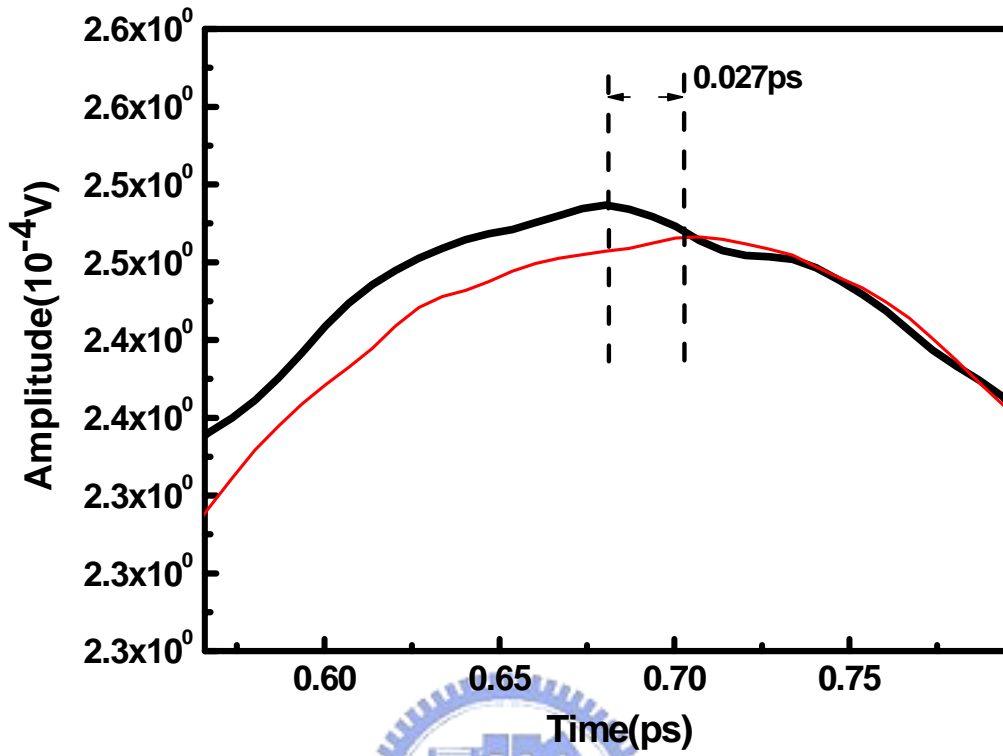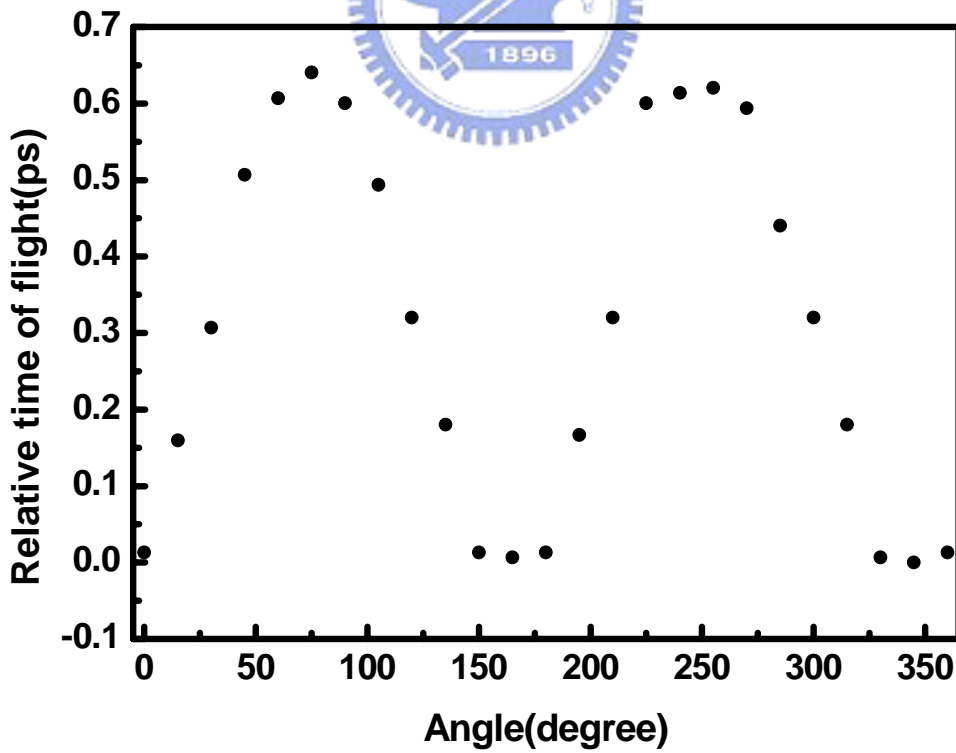
Fig. 4.14 Maximum disturbance of reference signal

Fig. 4.15 Relative time of flight of various angles of thicker sample

4.4 Transmission Spectroscopic Information of Hemoglobin

Fig. 4.16 is the transmission waveform of Hemoglobin (Hb) samples. THz radiation amplitude is decreased to about half of the reference THz waveform in case of the thin sample (320μm and 350μm). It is decreased to about 1/3 in case of the thick sample (960μm). Fig. 4.17 shows the FFT spectrum. Transmission spectrum amplitude is also larger in thin sample compared with the thick sample. Broadband absorption from 0.4THz to 2.0 THz has been observed in these deoxy-Hb samples. No special absorption line is found for powder or thin film hemoglobin, while broadband absorption from 0.4 to 2.0 THz is observed. THz transmittance spectrum of these Hb samples is calculated from spectrum amplitude of samples divided by the reference one, which is shown in Fig. 4.18. The transmission efficiency of thin Hb samples is gradually decreased as frequency increased which similar as the blood. However, it is dramatically decreased after 0.4THz in case of thick sample. It is even decreased to almost 0 after 1.4THz, which represents the strong absorption. In Fig. 4.19, the refractive index of powder and thin film sample is obvious different. Refractive indices of powders and thin film are from 1.88±0.01 to 1.83±0.01 and 1.73±0.05 to 1.60±0.05 with respectively from 0.2TH to 1.2THz. These are smaller than the blood case [15]. In Fig. 4.18, absorption coefficient of powders and thin film are from 3cm^{-1} to 33cm^{-1} and 8cm^{-1} to 39cm^{-1} with respectively from 0.2TH to 1.2THz. It is obviously smaller than value blood because of the less content of water absorption in these dry deoxcy-Hb samples.
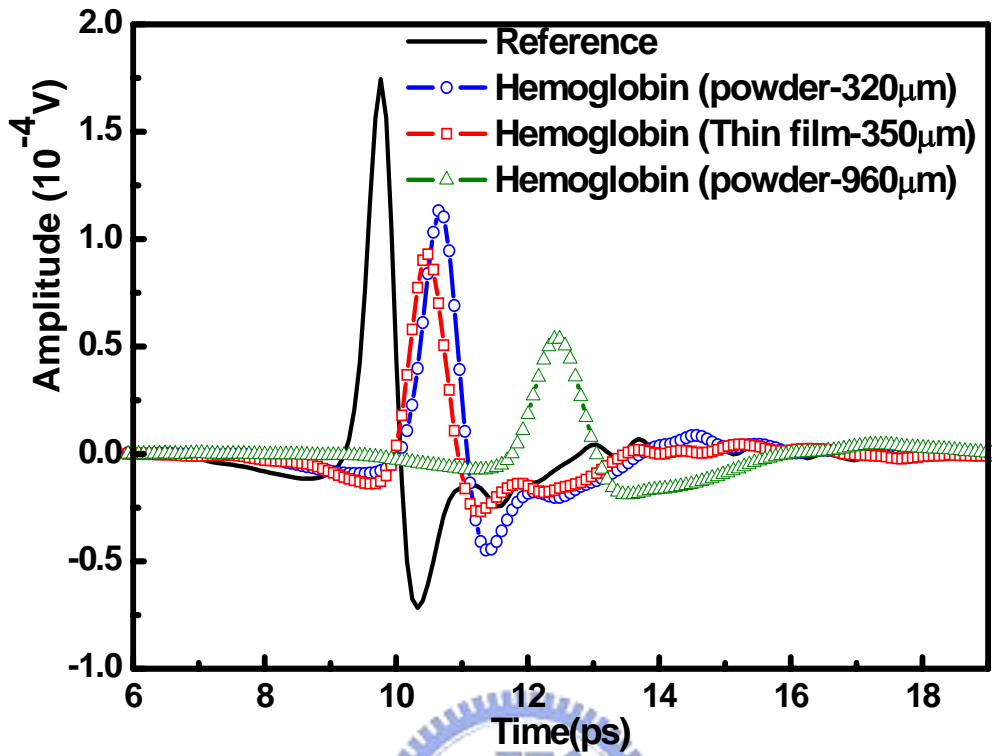
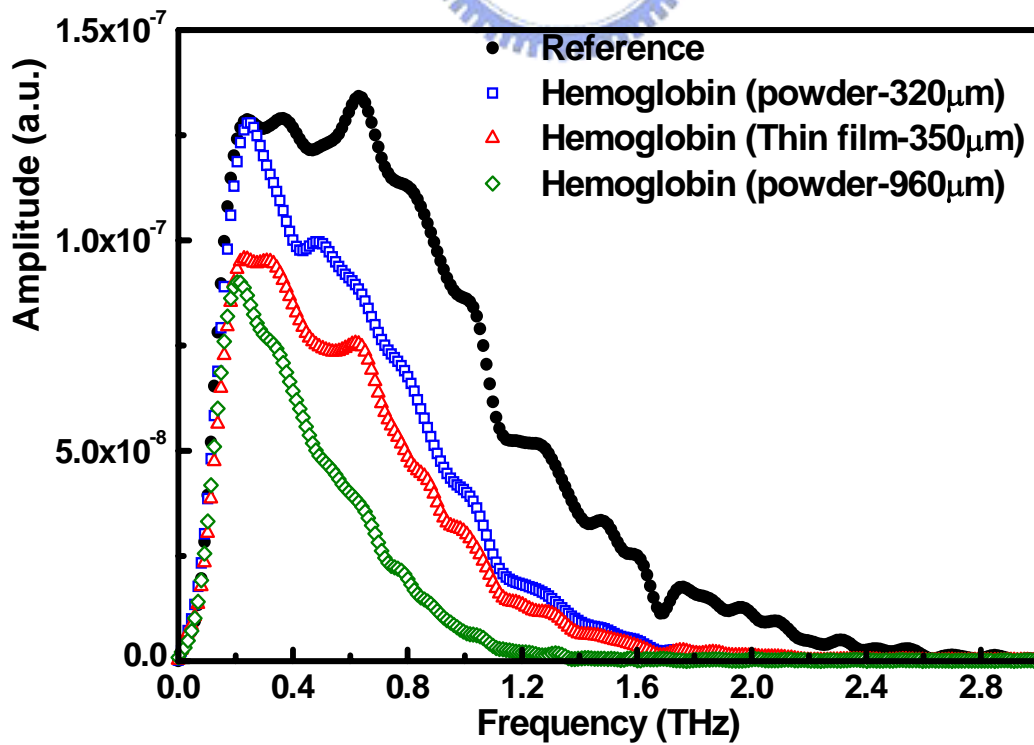Fig. 4.16 Waveform of transmitted THz signal

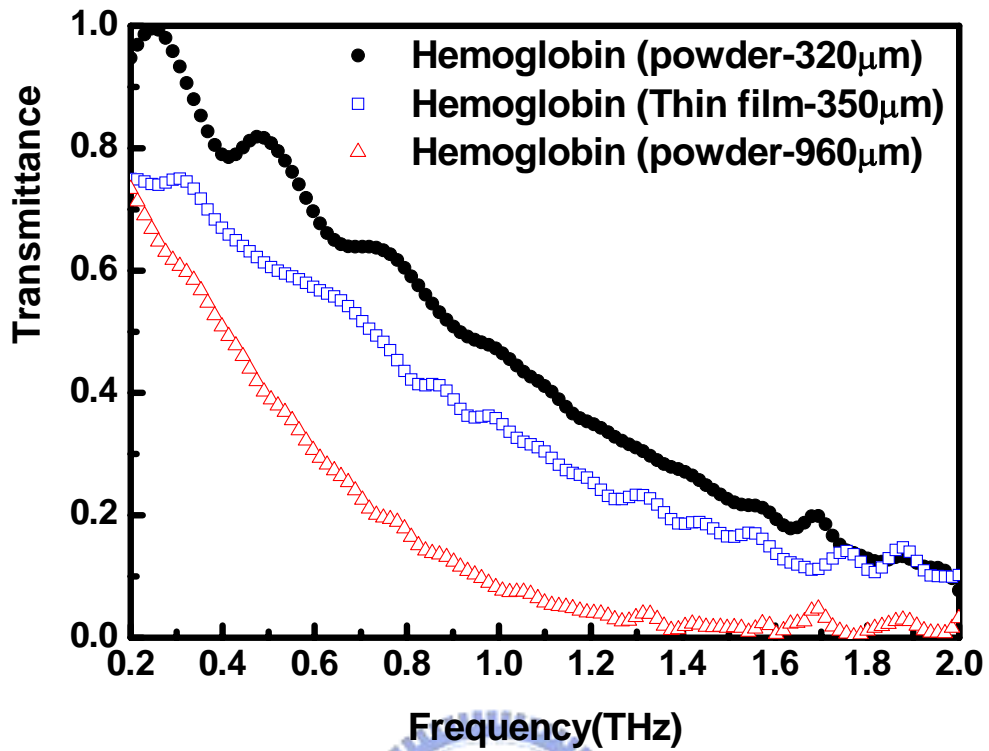Fig. 4.17 Spectrum of transmitted THz signal

38

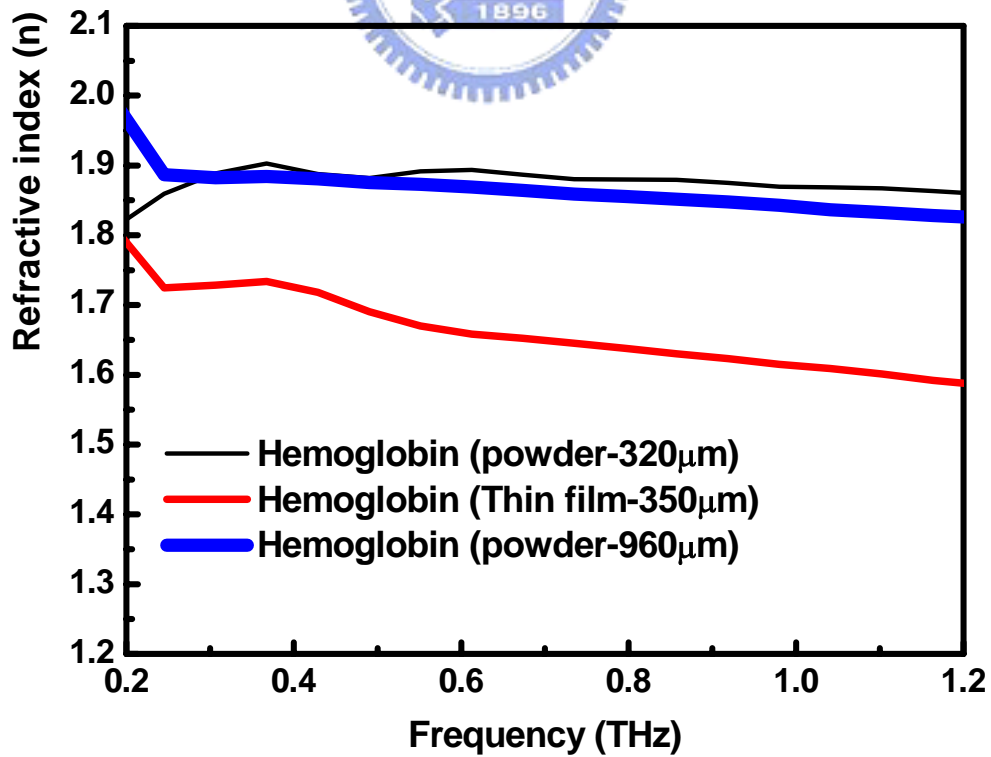Fig. 4.18 Transmittance of THz signal through hemoglobin

Fig. 4.19 Refractive index of hemoglobin from 0.2 THz to 1.2 THz
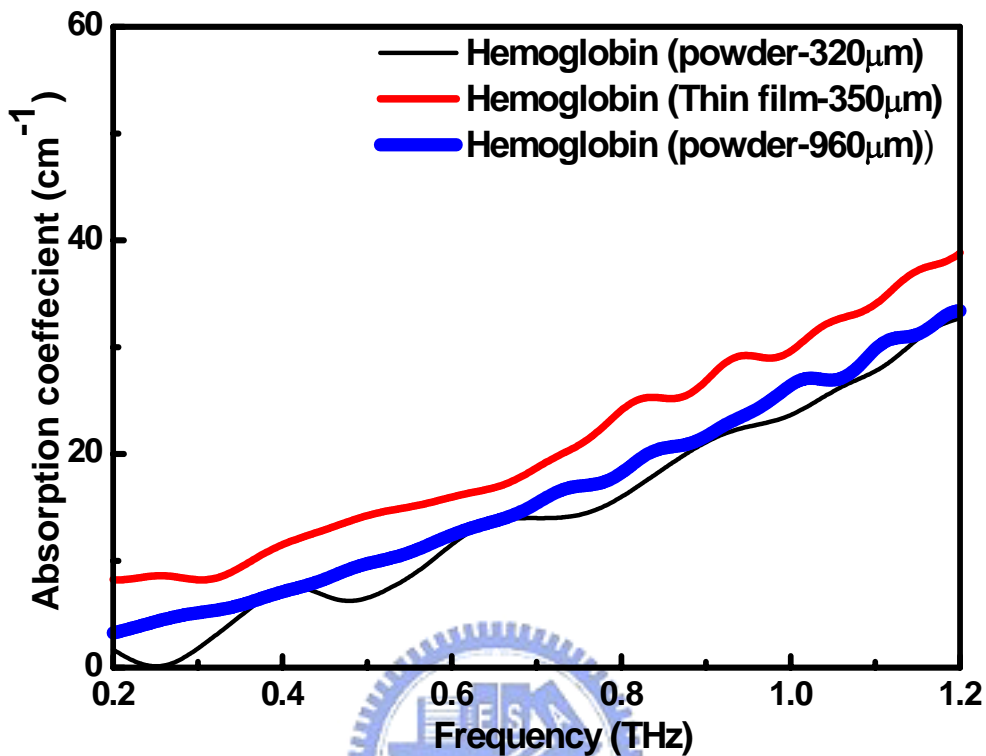
Fig. 4.20 Absorption coefficient of hemoglobin from 0.2 THz to 1.2 THz

4.5 Determination of Interface of Stacked Porcine Skins

From the experimental results of section 4.1 and section 4.2, the refractive indices of normal and burned porcine skins are different. This characteristic difference between normal and burned porcine skins makes it possible to detect the interface between burned and normal part of a partial burned skin. If the interface exists, wave propagates in the skin will be reflected and reflected signal can be detected to make sure the existence of burned-normal interface.

The reflected THz radiation of two layers porcine skins (burned porcine skin + normal porcine skin) is measured. The two layer structure

is applied to simply model the partially burned skin.

4.5.1 Reflected THz Waveform of One Layer of Porcine Skin

The reflected THz radiation of a normal porcine skin and a burned porcine skin is measured. The thicknesses of these two porcine skins are listed in Table 4.2.

	Normal	Burned
Thickness	0.27mm	0.53mm

Table 4.2 Thickness of porcine skins

Fig. 4.21 shows the expected conformation of the reflected THz waveform form single porcine skin. The measured waveform will be the superposition of the first and second reflected waveform.
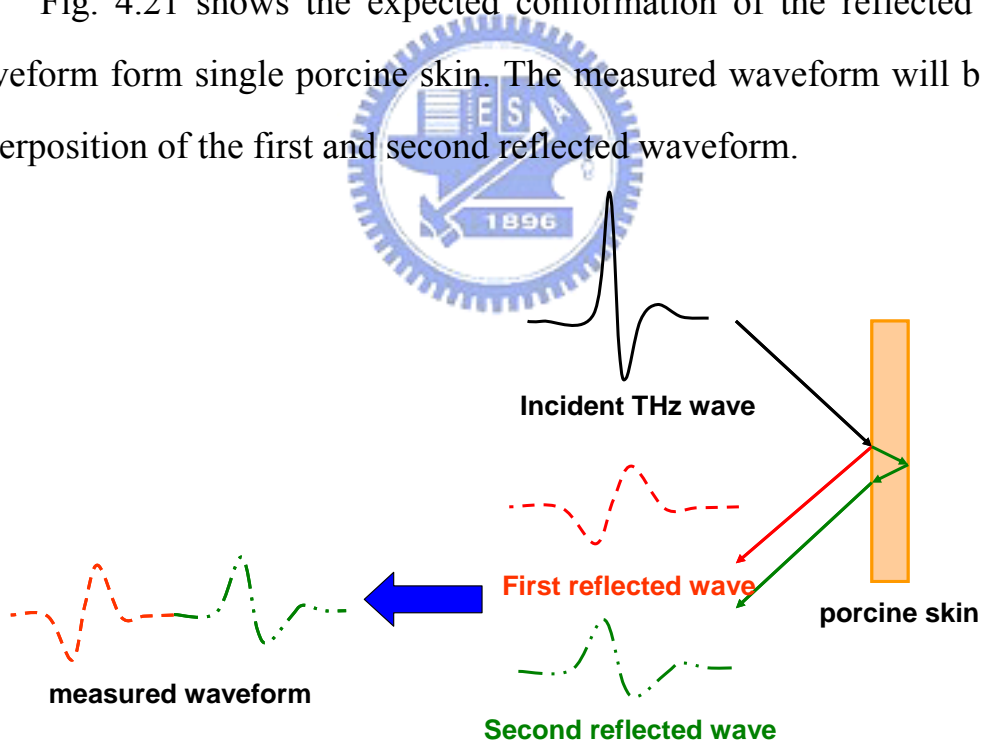
Fig. 4.21 Schematic of reflected THz waveform

From the measured results shown in Fig. 4.22 and Fig. 4.23, the reflected waveform is as expected as in Fig. 4.21. The times of flight

from first reflection to second reflection are 3.0 ps and 6.2 ps. The reflective indices of the normal and burned porcine skins are about 1.67 and 1.75 respectively.
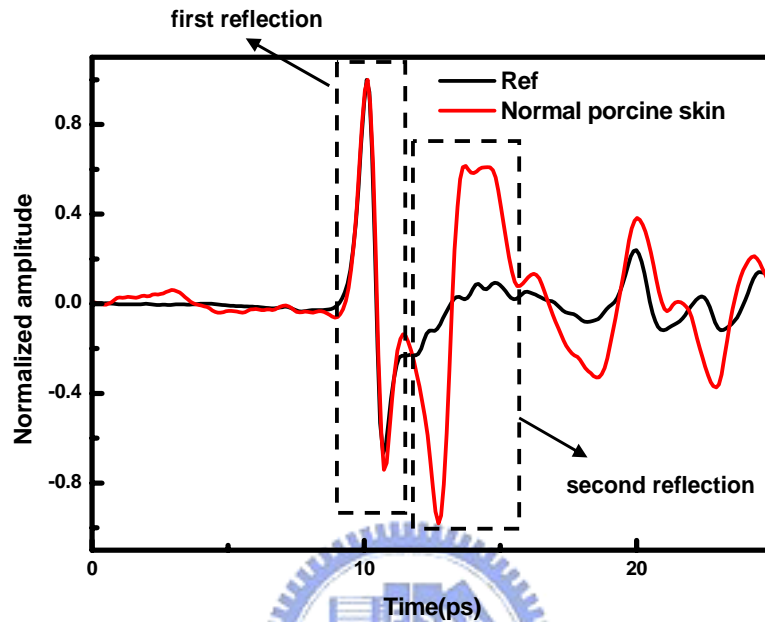

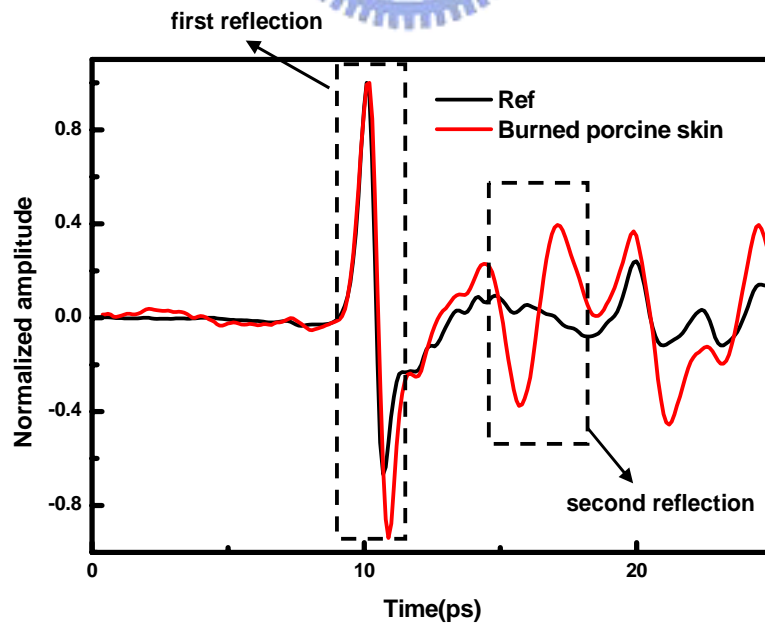Fig. 4.22 The reflected waveform of normal porcine skin

Fig. 4.23 The reflected waveform of burned porcine skin

4.5.2 Reflected THz Waveform of Two Layers of Stacked Porcine Skins

The normal and burned porcine skins are stacked to form the two layer structures. Fig. 4.24 shows the expected conformation of the reflected waveform from two stacked layers.
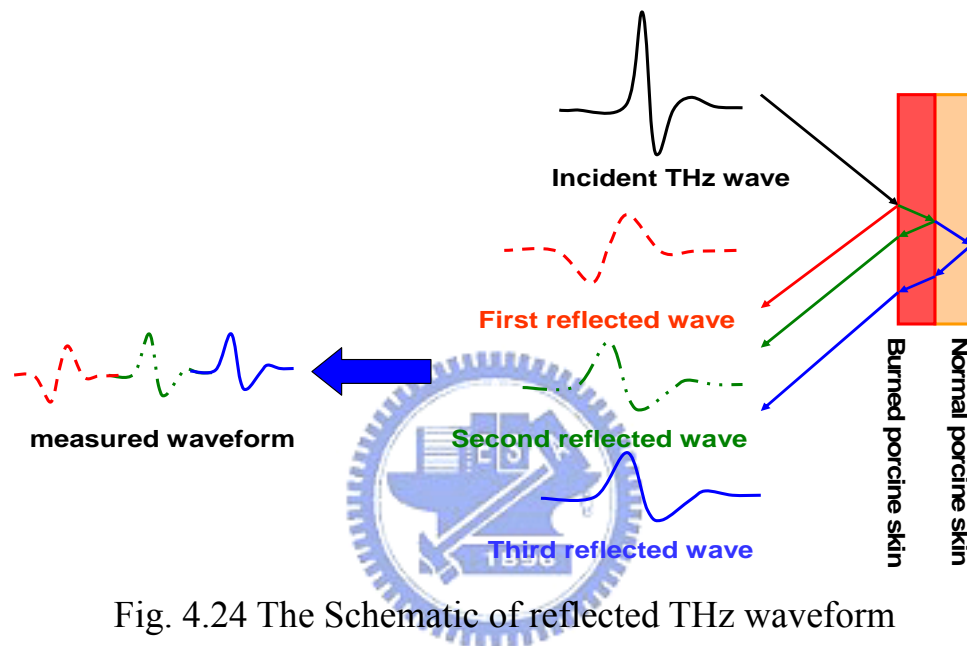
Fig. 4.24 The Schematic of reflected THz waveform

In Fig. 4.25, the first, second and third reflection THz waveforms are distinguished. The times of flight from first reflection to second reflection and second reflection to third reflection are 5.7 and 3.2 ps, which give the depth information about 488μm and 287μm respectively. The values of time of flight are very close to the results in section 4.5.1. There are several tenth μm of thickness differences in comparison with the measured thickness. The deviations of time of flight and thickness may caused from the surface of porcine is not very flat. The depth information of a simple burned-normal interface is detected from the measurement result.

Fig. 4.25 The reflected waveform of two layers of stacked porcine skins

5. Conclusions and Future Works

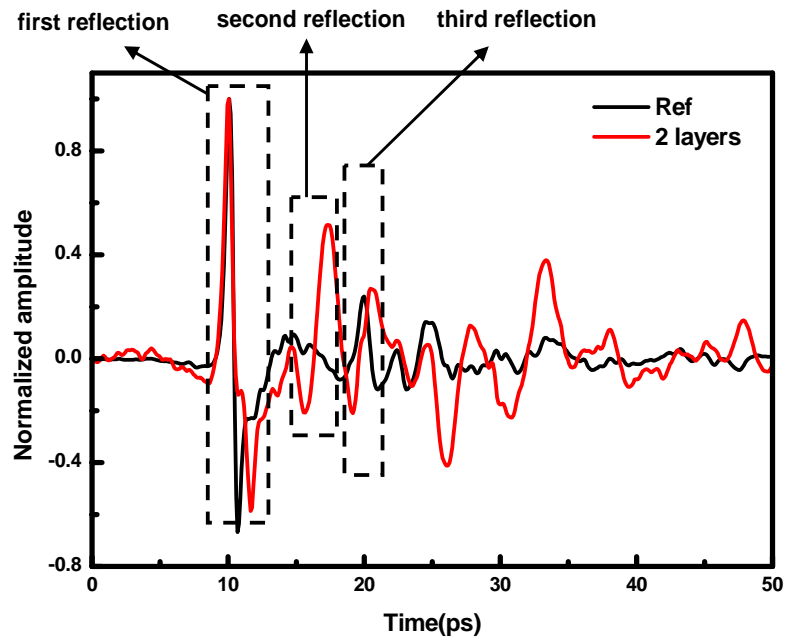In conclusion, the porcine skin has broadband absorption from 0.2 to 1.2THz. Difference in refractive indices of normal and burned porcine skins is found. The refractive index of normal porcine skin is from 1.77±0.01 to 1.66±0.01, which is smaller than the refractive index of burned porcine skin form 1.81±0.02 to 1.70±0.02 from 0.2THz to 1.0 THz. The absorption coefficients of normal and burned porcine skins are close. Furthermore, the reduction of birefringence between normal and burned porcine skin is observed. In addition, the spectroscopy of powder and thin-film hemoglobin is measured. Broadband absorption from 0.4THz to 2THz has been observed in hemoglobin samples. Refractive indices and absorption coefficients of hemoglobin have been demonstrated from 0.2THz to 1.2THz, which is important for the hemoglobin related biomedical-optics. Further reflective type measurement of the stacked burned and normal porcine skins for simulating partial burned biological skin can be implemented by THz -TDS. The waveform of THz radiation reflected from the surface, interface and back of the stacked structure of burned and normal porcine skins are resolved. Time of flight matched well with the original reflected waveform of normal and burned porcine skin. Clinical burned depth detection will be possible from these initial experiments.

In the future, THz-TDS will be further applied to the reflective type measurement of partial burned porcine skin to obtain the depth information. In addition, the spectroscopy of HbO_2 in the THz region will be measured.

Reference

[1] http://www.doh.gov.tw/statistic/index.htm

[2] http:// www.pride.hofstra.edu/~BCIAVA1/BURNS.HTM

[3] X-C Zhang, "Terahertz wave imaging: horizons and hurdles," *Phys. Med. Biol.*, Vol. 47, pp. 3667-3677, 2002

[4] Shyam M. Srinivas, Johannes F. de Boer, Hyle Park, Jun Zhang, Kourosh Keikhanzadeh et al, "Determination of burn depth by polarization-sensitive optical coherence tomography," *Journal of Biomedical Optics*, Vol. 9, No. 1, pp. 207-211, 2004

[5] Johannes F. de Boer, Shyam M. Srinivas, Arash Malekafzali, Zhongping Chen, J. Stuart Nelson, "Imaging thermally damaged tissue by polarization sensitive optical coherence tomography," *Opt. Express*, Vol. 3, No. 6, pp.212-218, 1998

[6] E. Pickwell, B E Cole, A J Fitzgerald, M Peeper, and V.P. Wallace, "In vivo study of human skin using pulsed terahertz radiation" *Phys. Med. Biol.* , Vol. 49 , pp. 1595-1607, 2004

[7] P.Y. Han, G.C. Cho, and X.-C. Zhang, "Time-domain transillumination of biological tissues with terahertz pulses" *Opt. Lett.*, Vol. **25**, pp. 242-244, 2000

[8] Cohen C, "Optical rotation and helical polypeptide chain configuration in collagen and gelatin," *J Biophys Biochem Cytol*, Vol. 1, No. 3, pp. 203-214, 1955

[9] Yoshioka K, O'Konski CT, "Electric properties of macromolecules. IX. Dipole moment, polarizability, and optical anisotropy factor of collagen in solution from electric birefringence," *Biopolymers*, Vol. 4, pp. 499-507, 1966

[10] Naylor EJ, "The structure of the corneas revealed by polarized light,"*Quart J Micr Sci*, Vol. 94, pp. 83-88, 1953

[11] van Blokland GJ, Verhelst SC, "Corneal polarization in the living human eye explained with a biaxial model," *J. Opt. Soc. Am. A*, Vol.4, pp. 82-90, 1987

[12] http://omlc.ogi.edu/spectra/hemoglobi

[13] D. J. Faber, M. C.G. Aalders, E. G. Mik, B. A. Hooper, M. J. C. van Gemert, and T. G. van Leeuwen, "Oxygen Saturation-Dependent Absorption and Scattering of Blood," *physical review letters*, Vol.**93**, pp. 28102-28105, 2004

[14] T. K. Das, Roy E. Weber, S. Dewilde, J. B. Wittenberg, B. A.

Wittenberg, K. Yamauchi, M.-L. Van Hauwaert, L. Moens, and D. L. Rousseau, "Ligand Binding in the Ferric and Ferrous States of Paramecium Hemoglobin, " *Biochemistry*, Vol.**39**, pp. 14330-14340, 2000

[15] A.J. Fitzgerald, E. Berry,N. N. Zinov'ev, S. H. Vanniasinkam, R. E. Miles, J. M. Chamberlain and M. A. Smith, "Catalogue of Human Tissue Optical Properties at Terahertz Frequencies," *Poster at Terahertz Bridge Workshop*, 2002

[16] A G Davies, E H Linfield and M B Johnston, " The development of t terahertz sources and their applications," Phys. Med. Biol., Vol. 47, pp. 3679-3689, 2002

[17] Y. Cai, I. Brener, J. Lopata, J. Wynn,L. Pfeiffer, and J.B. Stark et al, "Coherent Terahertz Radiation Detection: Direct Comparison between Free-space Electro-optic Sampling and Antenna Detection," *Applied Physics Letters*, Vol. 73, No. 4, pp.444~446, 1998

[18] Chamberlain J M, Miles R E, Collins C E, Steenson D P, "Introduction to Terahertz solid state sources," *New Direction of Terahertz Technology*, pp.3-27, 1997

[19] Wu Q, Zhang X C, "Free-Space Electro-Optic Sampling of Terahertz Beams," *Appl. Phys. Lett*, Vol. 67,pp. 3523-3525,1995.

[20] D. Dragoman, M. Dragoman, "Terahertz fields and applications," *Pro. in Quantum Electron.*, Vol. 28, No. 1, pp. 1-66, 2004

[21] Paul C. M. Planken, Han-Kwang, Huib J. Bakker et al, "Measurement and calculation of the orientation dependence of the terahertz pulse detection in ZnTe," *J. Opt. Soc. Am. B*, Vol. 18, No.3, pp.313-317, 2001

[22] S. Nashima, O. Morikawa, K. Takata, M. Hangyo, "Temperature dependence of optical and electronic properties of moderately doped silicon at terahertz frequencies," *J. Appl. Phys.*, Vol. 90, No. 2, 2001

[23] E. Pickwell, B. E. Cole, A. J. Fitzgerald, V. P. Wallace, M. Pepper, "Simulation of terahertz pulse propagation in biological systems," *Appl. Phys. Lett.*, Vol. 84, No. 12, pp. 2190-2192, 2004

[24] Duncan J. Maitland, Joseph T. Walsh, Jr.,"Quantitative Measurements of Linear Birefringence During Heating of Native Collagen," *Lasers in Surgery and Medicine*, Vol. 20, pp.310-318, 1997